A hybrid high-order locking-free method for linear elasticity on general meshes

Daniele Antonio Di Pietro, Alexandre Ern

A hybrid high-order locking-free method for linear elasticity on general meshes

Daniele A. Di Pietro*[1] and Alexandre Ern†[2]

[1] University of Montpellier 2, I3M, 34057 Montpellier CEDEX 5, France
[2]Université Paris-Est, CERMICS (ENPC), 6–8 avenue Blaise Pascal, 77455, Champs-sur-Marne, France

July 22, 2014

Abstract

We devise an arbitrary-order locking-free method for linear elasticity. The method relies on a pure-displacement (primal) formulation and leads to a symmetric, positive definite system matrix with compact stencil. The degrees of freedom are vector-valued polynomials of arbitrary order $k \geqslant 1$ on the mesh faces, so that in three space dimensions, the lowest-order scheme only requires 9 degrees of freedom per mesh face. The method can be deployed on general polyhedral meshes. The key idea is to reconstruct the symmetric gradient and divergence inside each mesh cell in terms of the degrees of freedom by solving inexpensive local problems. The discrete problem is assembled cell-wise using these operators and a high-order stabilization bilinear form. Locking-free error estimates are derived for the energy norm and for the L^2-norm of the displacement, with optimal convergence rates of order $(k+1)$ and $(k+2)$, respectively, for smooth solutions on general meshes. The theoretical results are confirmed numerically, and the CPU cost is evaluated on both standard and polygonal meshes.

Keywords Linear elasticity, general meshes, arbitrary order, locking-free methods

1 Introduction

Let $\Omega \subset \mathbb{R}^d$, $d \in \{2,3\}$, denote a bounded connected polygonal or polyhedral domain. We consider the isotropic linear elasticity problem

$$\begin{aligned} -\nabla\cdot\underline{\underline{\sigma}} &= \underline{f} && \text{in } \Omega \\ \underline{\underline{\sigma}} &= 2\mu\nabla_{\mathrm{s}}\underline{u} + \lambda(\nabla\cdot\underline{u})\underline{\underline{I}}_d && \text{in } \Omega, \\ \underline{u} &= \underline{0} && \text{on } \partial\Omega, \end{aligned} \tag{1}$$

with $\mu > 0$ and $\lambda \geqslant 0$ scalar Lamé coefficients and ∇_{s} denoting the symmetric part of the gradient operator (in short, the symmetric gradient) applied to vector-valued fields. We consider homogeneous Dirichlet boundary conditions on the displacement for simplicity. More

*daniele.di-pietro@univ-montp2.fr, corresponding author
†ern@cermics.enpc.fr

general boundary conditions can be handled. For $X \subset \overline{\Omega}$, we denote by $(\cdot,\cdot)_X$ and $\|\cdot\|_X$ respectively the standard inner product and norm of $L^2(X)$, with the convention that the index is omitted if $X = \Omega$. A similar notation is used for $L^2(X)^d$ and $L^2(X)^{d\times d}$. With $\underline{f} \in L^2(\Omega)^d$, the weak formulation of problem (1) consists in finding $\underline{u} \in \underline{U}_0 := H^1_0(\Omega)^d$ such that, for all $\underline{v} \in \underline{U}_0$,

$$(2\mu\nabla_{\rm s}\underline{u}, \nabla_{\rm s}\underline{v}) + (\lambda\nabla\cdot\underline{u}, \nabla\cdot\underline{v}) = (\underline{f}, \underline{v}). \tag{2}$$

It is known that the accurate approximation of problem (2) in the incompressible limit $\lambda \to +\infty$ requires the discrete space to be able to accurately represent nontrivial divergence-free vector-valued fields. When considering primal approximations where the displacement field is the sole unknown, this essentially amounts to having at hand a divergence operator that satisfies a suitable commuting diagram property. Combined with the regularity result on the displacement field and its divergence (see Eq. (45) below), the commuting diagram property allows one to prove error estimates that are uniform with respect to λ. In the work of Brenner and Sung [8], this property is obtained for the pure-displacement problem using the nonconforming element of Crouzeix and Raviart [10] and the Navier–Cauchy formulation. It is also possible to penalize the jumps of the discrete displacement field across interfaces in a least-squares fashion, as do Hansbo and Larson [20].

All of the above-mentioned approaches apply to standard simplicial or parallelepipedal meshes. In recent years, a large effort has been devoted to the development and analysis of discretization methods that apply to more general meshes possibly featuring polygonal or polyhedral elements and nonconforming interfaces. In this context, we mention the lowest-order method of Beirão da Veiga, Gyrya, Lipnikov, and Manzini [5] for Stokes flow and that of Beirão da Veiga [6] for mixed linear elasticity, and the work of Di Pietro and Lemaire [16], which introduces a generalization of the lowest-order Crouzeix–Raviart space and, correspondingly, of the methods of [8, 20]. Closer to the classical finite element spirit is the work of Tabarraei and Sukumar [28], where Lagrangian shape functions for convex polygonal elements are constructed. More recently, arbitrary-order methods on general meshes have received an increasing attention. We cite here, in particular, the work of Beirão da Veiga, Brezzi, and Marini [4], where the authors introduce a locking-free Virtual Element method for planar linear elasticity featuring vertex, edge, and element unknowns.

In this work, we devise a new approach to designing an arbitrary-order method for quasi-incompressible linear elasticity on general meshes in space dimension $d \in \{2, 3\}$ based on the recent ideas of [13, 14] for diffusive problems. For a polynomial degree $k \geqslant 1$, our starting point is to consider as degrees of freedom (DOFs) vector-valued polynomials at mesh elements and faces up to degree k. The design of the method then proceeds in two steps: (i) we introduce discrete symmetric gradient and divergence reconstruction operators hinging on the solution of inexpensive local problems inside each mesh element, in such a way that the discrete divergence operator satisfies the commuting diagram property; (ii) we devise a least-squares stabilization that weakly enforces the matching of element- and face-based DOFs. The global system is assembled cell-wise using the above local reconstruction and stabilization operators. Face-based DOFs establish inter-element connections at interfaces and can be used to strongly enforce essential boundary conditions at boundary faces. Element-based DOFs are intermediate variables which can be eliminated by static condensation from the global system. Hence, DOFs in the global system are vector-valued polynomials of order $k \geqslant 1$ on the mesh faces. For instance, the lowest-order scheme only requires 9 degrees of freedom per mesh face in 3 space dimensions.

Discretization schemes for elliptic problems using face-based DOFs have received an increasing attention in the last few years. We mention the seminal work of Cockburn, Gopalakrishnan, and Lazarov [9] on Hybrid Discontinuous Galerkin (HDG) and the more recent works of Wang and Ye [29] on the Weak Galerkin (WG) method, that of Lipnikov and Manzini on Mimetic Finite Differences (MFD) [25], and that of the authors on Hybrid High-Order (HHO) schemes [13, 14]. Although HDG and WG methods also reconstruct operators inside each element, there are two important differences with HHO methods. First, the spaces in which we reconstruct the symmetric gradient are not just tensor-valued polynomials, but the image of vector-valued polynomials by the continuous symmetric gradient operator. This allows us to define a higher-order displacement reconstruction operator which constitutes the main ingredient of the second distinctive feature, namely the design of the stabilization bilinear form. This design is by no means straightforward, since the stabilization (i) remains local to each element; (ii) ensures coercivity; (iii) yields optimal (higher-order) approximation properties. We also mention that among the above schemes, only HDG schemes have been, to our knowledge, devised for linear elasticity; we refer, e.g., to Soon, Cockburn, and Stolarski [27] where various choices of the reconstruction spaces (which differ from HHO) are discussed.

The present HHO method exhibits various salient benefits. The method (i) relies on a pure-displacement (primal) formulation, thereby leading to a symmetric, positive definite system matrix and to strongly symmetric strain and stress tensors; (ii) is computationally effective since the use of face unknowns (and the absence of nodal unknowns) yields a compact stencil (consisting of face neighbors in the sense of faces) and greatly simplifies data exchange (especially in three space dimensions); (iii) leads, for smooth solutions, to optimal, locking-free strain and displacement error estimates of order $(k+1)$ and $(k+2)$, respectively, on general polyhedral meshes. The price to pay is twofold. First, local problems related to the reconstruction operators have to be solved. Our numerical results indicate that the associated cost quickly becomes marginal with respect to the cost of solving the global system as the number of DOFs is increased. Second, the method is nonconforming, so that, for instance, the displacement can be multi-valued at a mesh vertex; however, displacement jumps optimally converge to zero as the mesh is refined. As a result, any standard post-processing operator (e.g., by local nodal averages) can be used to produce a conforming displacement field.

The paper is organized as follows. In Section 2, we recall the definition of admissible mesh sequences in the spirit of [12] as well as some useful results. In Section 3, we introduce the local DOFs, the local reduction map (mapping continuous functions to DOFs) and the symmetric gradient and divergence reconstruction operators (mapping DOFs to polynomial functions), and identify the key properties of these operators. In Section 4, we define the stabilized discrete bilinear form, state the discrete problem, and show its well-posedness. In Section 5, we perform the error analysis and prove locking-free error estimates of order $(k+1)$ in the energy norm and $(k+2)$ in the L^2-norm for smooth solutions. In Section 6, we discuss implementation aspects, present numerical examples on polygonal meshes confirming our theoretical results, and evaluate the efficiency of the proposed method in terms of CPU cost.

2 Setting

2.1 Admissible mesh sequences

In this section we briefly recall the notion of admissible mesh sequence of [12, Chapter 1]. Let $\mathcal{H} \subset \mathbb{R}_*^+$ denote a countable set of meshsizes having 0 as its unique accumulation point.

We focus on sequences $(\mathcal{T}_h)_{h\in\mathcal{H}}$ where, for all $h \in \mathcal{H}$, $\mathcal{T}_h$ is a finite collection of nonempty disjoint open polyhedra (called elements or cells) $\mathcal{T}_h = \{T\}$ such that $\overline{\Omega} = \bigcup_{T\in\mathcal{T}_h} \overline{T}$ and $h = \max_{T\in\mathcal{T}_h} h_T$ (h_T stands for the diameter of T). A hyperplanar closed connected subset F of $\overline{\Omega}$ is called a face if it has positive $(d-1)$-dimensional measure and (i) either there exist $T_1, T_2 \in \mathcal{T}_h$ such that $F = \partial T_1 \cap \partial T_2$ (and F is an interface) or (ii) there exists $T \in \mathcal{T}_h$ such that $F = \partial T \cap \partial\Omega$ (and F is a boundary face). The set of interfaces is denoted by $\mathcal{F}_h^{\mathrm{i}}$, the set of boundary faces by $\mathcal{F}_h^{\mathrm{b}}$, and we let $\mathcal{F}_h := \mathcal{F}_h^{\mathrm{i}} \cup \mathcal{F}_h^{\mathrm{b}}$. The diameter of a face $F \in \mathcal{F}_h$ is denoted by h_F. For all $T \in \mathcal{T}_h$, $\mathcal{F}_T := \{F \in \mathcal{F}_h \mid F \subset \partial T\}$ denotes the set of faces lying on the boundary of T and, for all $F \in \mathcal{F}_T$, we denote by $\underline{n}_{TF}$ the normal to F pointing out of T. The m-dimensional Lebesgue measure, $m \in \{0 \dots d\}$, is denoted by $|\cdot|_m$.

Definition 1 (Admissible mesh sequence)**.** *We say that the mesh sequence $(\mathcal{T}_h)_{h\in\mathcal{H}}$ is admissible if, for all $h \in \mathcal{H}$, $\mathcal{T}_h$ admits a matching simplicial submesh $\mathfrak{T}_h$ (so that any cell (resp., face) of $\mathfrak{T}_h$ is a subset of a cell (resp., face) of $\mathcal{T}_h$) and there exists a real number $\varrho > 0$ (the mesh regularity parameter) independent of h such that the following conditions hold: (i) for all $h \in \mathcal{H}$ and all simplex $S \in \mathfrak{T}_h$ of diameter h_S and inradius r_S, $\varrho h_S \leqslant r_S$ (shape-regularity) and (ii) for all $h \in \mathcal{H}$, all $T \in \mathcal{T}_h$, and all $S \in \mathfrak{T}_h$ such that $S \subset T$, $\varrho h_T \leqslant h_S$ (contact-regularity).*

In what follows, we consider meshes belonging to an admissible mesh sequence. We recall two useful geometric results that hold in this framework. Owing to [12, Lemma 1.42], for all $h \in \mathcal{H}$, all $T \in \mathcal{T}_h$, and all $F \in \mathcal{F}_T$, h_F is comparable to h_T in the sense that

$$\varrho^2 h_T \leqslant h_F \leqslant h_T. \tag{3}$$

Moreover, owing to [12, Lemma 1.41], there exists an integer $N_\partial \geqslant (d+1)$ (depending on ϱ) such that the maximum number of faces of one element is bounded,

$$\forall h \in \mathcal{H}, \qquad \max_{T\in\mathcal{T}_h} \mathrm{card}(\mathcal{F}_T) \leqslant N_\partial. \tag{4}$$

In what follows, we often abbreviate as $a \lesssim b$ the inequality $a \leqslant Cb$ with $C > 0$ independent of h, μ, and λ, but possibly depending on the mesh-regularity parameter ϱ. Tracking the dependence on Lamé's parameters of the constant appearing in the inequalities allows one to investigate the properties of the method in the incompressible limit.

2.2 Basic results

In this section we recall some basic results on admissible mesh sequences. There exist real numbers C_{tr} and $C_{\mathrm{tr,c}}$ depending on ϱ but independent of h such that the following discrete trace inequalities hold for all $T \in \mathcal{T}_h$, cf. [12, Lemmata 1.46 and 1.49]:

$$\|v\|_F \leqslant C_{\mathrm{tr}} h_F^{-1/2} \|v\|_T \qquad \forall v \in \mathbb{P}_d^l(T),\ \forall F \in \mathcal{F}_T, \tag{5}$$

$$\|v\|_{\partial T} \leqslant C_{\mathrm{tr,c}} \big(h_T^{-1}\|v\|_T^2 + h_T\|\nabla v\|_T^2\big)^{1/2} \qquad \forall v \in H^1(T), \tag{6}$$

where $\mathbb{P}_d^l(T)$ denotes the space spanned by the restrictions to T of d-variate polynomials of total degree $\leqslant l$. Using [12, Lemma 1.40] together with the results of [18], it can be proved that there exists a real number C_{app} depending on ϱ but independent of h such that, for all $T \in \mathcal{T}_h$, denoting by π_T^l the L^2-orthogonal projector on $\mathbb{P}_d^l(T)$, the following inequality holds: For all $T \in \mathcal{T}_h$, all $s \in \{1, \dots, (l+1)\}$, and all $v \in H^s(T)$,

$$|v - \pi_T^l v|_{H^m(T)} + h_T^{1/2}|v - \pi_T^l v|_{H^m(\partial T)} \leqslant C_{\mathrm{app}} h_T^{s-m} |v|_{H^s(T)} \qquad \forall m \in \{0, \dots, (s-1)\}. \tag{7}$$

The following Poincaré inequality is valid for all $T \in \mathcal{T}_h$ and all $v \in H^1(T)$ such that $\int_T v = 0$:

$$\|v\|_T \leqslant C_{\mathrm{P}} h_T \|\nabla v\|_T, \tag{8}$$

where $C_{\mathrm{P}} = \pi^{-1}$ for convex elements (cf. [3]), while, for more general element shapes, C_{P} can be estimated in terms of the mesh-regularity parameter ϱ. For all $T \in \mathcal{T}_h$, we set

$$\underline{\mathcal{U}}(T) := \left\{ \underline{v} \in H^1(T)^d \mid \int_T \underline{v} = \underline{0} \text{ and } \int_T \nabla_{\mathrm{ss}} \underline{v} = \underline{\underline{0}} \right\}, \tag{9}$$

where ∇_{ss} denotes the skew-symmetric part of the gradient operator. The following second Korn inequality holds for all $T \in \mathcal{T}_h$ and all $\underline{v} \in \underline{\mathcal{U}}(T)$:

$$\|\nabla \underline{v}\|_T \leqslant C_{\mathrm{K},2} \|\nabla_{\mathrm{s}} \underline{v}\|_T, \tag{10}$$

where $C_{\mathrm{K},2} > 0$ is independent of h and can be estimated in terms of the mesh-regularity parameter ϱ, cf., e.g., [24, 22, 23] for the two-dimensional case. Combining (8) and (10), we infer that, for all $T \in \mathcal{T}_h$ and all $\underline{v} \in \underline{\mathcal{U}}(T)$,

$$\|\underline{v}\|_T \leqslant C_{\mathrm{K}} h_T \|\nabla_{\mathrm{s}} \underline{v}\|_T, \tag{11}$$

with $C_{\mathrm{K}} = C_{\mathrm{K},2} C_{\mathrm{P}}$. The bound (11) also holds if $\underline{v} \in H^1(T)^d$ and there exists $\Gamma \subset \partial T$ with $|\Gamma|_{d-1} \neq 0$ such that $\underline{v}_{|\Gamma} = \underline{0}$.

3 Local reconstruction operators

In this section we define the local DOFs, the local reduction map, and the local symmetric gradient and divergence reconstruction operators.

3.1 Degrees of freedom and reduction map

Let a polynomial degree $k \geqslant 0$ be fixed. For all $T \in \mathcal{T}_h$, we define the local space of DOFs as

$$\underline{\mathsf{U}}_T^k := \mathbb{P}_d^k(T)^d \times \left\{ \bigtimes_{F \in \mathcal{F}_T} \mathbb{P}_{d-1}^k(F)^d \right\}. \tag{12}$$

For $\underline{\mathsf{v}} \in \underline{\mathsf{U}}_T^k$, we use the notation $\underline{\mathsf{v}} = (\underline{\mathsf{v}}_T, (\underline{\mathsf{v}}_F)_{F \in \mathcal{F}_T})$. The degrees of freedom are illustrated in Figure 1 for $k = 1$ and $k = 2$. The local reduction map $I_T^k : \underline{U}(T) := H^1(T)^d \to \underline{\mathsf{U}}_T^k$ is such that, for all $\underline{v} \in \underline{U}(T)$,

$$I_T^k \underline{v} = (\pi_T^k \underline{v}, (\pi_F^k \underline{v})_{F \in \mathcal{F}_T}). \tag{13}$$

3.2 Symmetric gradient

Let $T \in \mathcal{T}_h$. We first define a local displacement reconstruction operator $\underline{r}_T^k : \underline{\mathsf{U}}_T^k \to \mathbb{P}_d^{k+1}(T)^d$. For given DOFs $\underline{\mathsf{v}} = (\underline{\mathsf{v}}_T, (\underline{\mathsf{v}}_F)_{F \in \mathcal{F}_T}) \in \underline{\mathsf{U}}_T^k$, the field $\underline{r}_T^k \underline{\mathsf{v}} \in \mathbb{P}_d^{k+1}(T)^d$ is defined by solving the following well-posed pure-traction problem in T: For all $\underline{w} \in \mathbb{P}_d^{k+1}(T)^d$,

$$(\nabla_{\mathrm{s}}(\underline{r}_T^k \underline{\mathsf{v}}), \nabla_{\mathrm{s}} \underline{w})_T = (\nabla_{\mathrm{s}} \underline{\mathsf{v}}_T, \nabla_{\mathrm{s}} \underline{w})_T + \sum_{F \in \mathcal{F}_T} (\underline{\mathsf{v}}_F - \underline{\mathsf{v}}_T, \nabla_{\mathrm{s}} \underline{w} \underline{n}_{TF})_F. \tag{14}$$

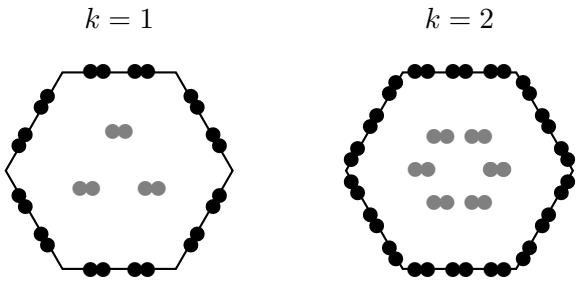

Figure 1: Face (black) and cell (grey) degrees of freedom in $\underline{\mathsf{U}}_T^k$ (cf. (12)) for $k=1$ and $k=2$. Cell degrees of freedom can be locally eliminated via static condensation.

This linear system is of size $d\binom{k+1+d}{k+1}$ (e.g., for $k=1$, leading to a quadratic reconstruction, the local system is of size 12 if $d=2$ and 30 if $d=3$). The solvability of (14) stems from the fact that the right-hand side vanishes if the test function $\underline{w}$ is a rigid-body motion. The solution to (14) is uniquely defined if we prescribe the rigid-body motion components of $\underline{r}_T^k\underline{\mathsf{v}}$, and we choose the following prescription:

$$\int_T \underline{r}_T^k\underline{\mathsf{v}} = \int_T \underline{\mathsf{v}}_T, \qquad \int_T \nabla_{\mathrm{ss}}(\underline{r}_T^k\underline{\mathsf{v}}) = \sum_{F\in\mathcal{F}_T}\int_F \frac{1}{2}(\underline{n}_{TF}\otimes\underline{\mathsf{v}}_F - \underline{\mathsf{v}}_F\otimes\underline{n}_{TF}), \tag{15}$$

which ensures that $(\underline{r}_T^k I_T^k\underline{v}-\underline{v})\in\underline{\mathcal{U}}(T)$ for all $\underline{v}\in\underline{\mathsf{U}}_T^k$ (as shown in the proof of Lemma 2 below). We then define the local discrete symmetric gradient operator $\underline{\underline{E}}_T^k:\underline{\mathsf{U}}_T^k\to\nabla_{\mathrm{s}}\mathbb{P}_d^{k+1}(T)^d$ such that

$$\underline{\underline{E}}_T^k\underline{\mathsf{v}} := \nabla_{\mathrm{s}}(\underline{r}_T^k\underline{\mathsf{v}}). \tag{16}$$

Owing to (16), we infer that, for all $\underline{w}\in\mathbb{P}_d^{k+1}(T)^d$,

$$(\underline{\underline{E}}_T^k\underline{\mathsf{v}},\nabla_{\mathrm{s}}\underline{w})_T := (\nabla_{\mathrm{s}}\underline{\mathsf{v}}_T,\nabla_{\mathrm{s}}\underline{w})_T + \sum_{F\in\mathcal{F}_T}(\underline{\mathsf{v}}_F-\underline{\mathsf{v}}_T,\nabla_{\mathrm{s}}\underline{w}\,\underline{n}_{TF})_F \tag{17a}$$

$$= -(\underline{\mathsf{v}}_T,\nabla\cdot\nabla_{\mathrm{s}}\underline{w})_T + \sum_{F\in\mathcal{F}_T}(\underline{\mathsf{v}}_F,\nabla_{\mathrm{s}}\underline{w}\,\underline{n}_{TF})_F, \tag{17b}$$

where the second equation follows by integrating by parts. The composition of the reduction map by the displacement reconstruction operator yields an approximation operator $\underline{r}_T^k I_T^k : \underline{U}(T)\to\mathbb{P}_d^{k+1}(T)^d$ mapping continuous functions to polynomials in T. We now study the approximation properties of this operator on smooth functions.

Lemma 2 (Approximation properties for $\underline{r}_T^k I_T^k$)**.** *Let $k\geqslant 0$ and $T\in\mathcal{T}_h$. There exists a real number $C>0$ depending on ϱ and k, but independent of h, such that, for all $\underline{v}\in H^{k+2}(T)^d$,*

$$\begin{aligned}\|\underline{r}_T^k I_T^k\underline{v}-\underline{v}\|_T + h_T^{1/2}\|\underline{r}_T^k I_T^k\underline{v}-\underline{v}\|_{\partial T}\\ + h_T\|\nabla_{\mathrm{s}}(\underline{r}_T^k I_T^k\underline{v}-\underline{v})\|_T + h_T^{3/2}\|\nabla_{\mathrm{s}}(\underline{r}_T^k I_T^k\underline{v}-\underline{v})\|_{\partial T} \leqslant Ch_T^{k+2}\|\underline{v}\|_{H^{k+2}(T)^d}.\end{aligned} \tag{18}$$

Proof. (1) Let $\underline{v}\in H^{k+2}(T)^d$. Using the definitions (14) of $\underline{r}_T^k$ and (13) of I_T^k, we infer that,

for all $\underline{w} \in \mathbb{P}_d^{k+1}(T)^d$,

$$(\nabla_{\rm s}\underline{r}_T^k I_T^k \underline{v}, \nabla_{\rm s}\underline{w})_T = -(\pi_T^k \underline{v}, \nabla\cdot\nabla_{\rm s}\underline{w})_T + \sum_{F\in\mathcal{F}_T} (\pi_F^k \underline{v}, \nabla_{\rm s}\underline{w}\underline{n}_{TF})_F$$
$$= -(\underline{v}, \nabla\cdot\nabla_{\rm s}\underline{w})_T + \sum_{F\in\mathcal{F}_T} (\underline{v}, \nabla_{\rm s}\underline{w}\underline{n}_{TF})_F,$$

since $\nabla\cdot\nabla_{\rm s}\underline{w} \in \mathbb{P}_d^{k-1}(T)^d \subset \mathbb{P}_d^k(T)^d$ and $(\nabla_{\rm s}\underline{w})_{|F}\underline{n}_{TF} \in \mathbb{P}_{d-1}^k(F)^d$. Integrating by parts the right-hand side yields

$$(\nabla_{\rm s}\underline{r}_T^k I_T^k \underline{v} - \nabla_{\rm s}\underline{v}, \nabla_{\rm s}\underline{w})_T = 0 \qquad \forall \underline{w} \in \mathbb{P}_d^{k+1}(T)^d. \tag{19}$$

The orthogonality condition (19) implies that

$$\|\nabla_{\rm s}(\underline{r}_T^k I_T^k \underline{v} - \underline{v})\|_T = \inf_{\underline{w}\in\mathbb{P}_d^{k+1}(T)^d} \|\nabla_{\rm s}(\underline{w} - \underline{v})\|_T \lesssim h_T^{k+1}\|\underline{v}\|_{H^{k+2}(T)^d}, \tag{20}$$

where the last inequality follows from the approximation property (7) of π_T^{k+1} (with $s = k+2$ and $m = 1$).

(2) Let us now verify that $\underline{r}_T^k I_T^k \underline{v} - \underline{v} \in \underline{\mathcal{U}}(T)$. We first observe that, owing to (15), $\int_T \underline{r}_T^k I_T^k \underline{v} = \int_T \pi_T^k \underline{v} = \int_T \underline{v}$. In addition,

$$\int_T \nabla_{\rm ss}(\underline{r}_T^k I_T^k \underline{v}) = \sum_{F\in\mathcal{F}_T} \int_F \frac{1}{2}(\underline{n}_{TF}\otimes\pi_F^k\underline{v} - \pi_F^k\underline{v}\otimes\underline{n}_{TF})$$
$$= \sum_{F\in\mathcal{F}_T} \int_F \frac{1}{2}(\underline{n}_{TF}\otimes\underline{v} - \underline{v}\otimes\underline{n}_{TF}) = \int_T \nabla_{\rm ss}\underline{v}.$$

As a result, using Korn's inequality (11), together with (20), we infer that

$$\|\underline{r}_T^k I_T^k \underline{v} - \underline{v}\|_T \lesssim h_T\|\nabla_{\rm s}(\underline{r}_T^k I_T^k \underline{v} - \underline{v})\|_T \lesssim h_T^{k+2}\|\underline{v}\|_{H^{k+2}(T)^d}. \tag{21}$$

(3) Using the continuous trace inequality (6) followed by Korn's inequality (10), together with (20) and (21), we infer that

$$h_T\|\underline{r}_T^k I_T^k \underline{v} - \underline{v}\|_{\partial T}^2 \lesssim \|\underline{r}_T^k I_T^k \underline{v} - \underline{v}\|_T^2 + h_T^2\|\nabla_{\rm s}(\underline{r}_T^k I_T^k \underline{v} - \underline{v})\|_T^2 \lesssim h_T^{2(k+1)}\|\underline{v}\|_{H^{k+2}(T)^d}^2. \tag{22}$$

Finally, the bound on $h_T^{3/2}\|\nabla_{\rm s}(\underline{r}_T^k I_T^k \underline{v} - \underline{v})\|_{\partial T}$ is obtained by introducing $\pm\pi_T^k\nabla_{\rm s}\underline{v}$ inside the norm and using the triangle inequality, the approximation property (7) of π_T^k (applied componentwise to $\nabla_{\rm s}\underline{v}$ with $s = k+1$ and $m = 0$), the discrete trace inequality (5), the bound (4) on $\mathrm{card}(\mathcal{F}_T)$, the mesh regularity property (3), the fact that $\nabla_{\rm s}\underline{r}_T^k I_T^k \underline{v} \in \mathbb{P}_d^k(T)^{d\times d}$ so that $\|\pi_T^k\nabla_{\rm s}\underline{v} - \nabla_{\rm s}\underline{r}_T^k I_T^k \underline{v}\|_T \leqslant \|\nabla_{\rm s}(\underline{v} - \underline{r}_T^k I_T^k \underline{v})\|_T$, and (20). □

3.3 Divergence

Let $T \in \mathcal{T}_h$. The local discrete divergence operator $D_T^k : \underline{\mathsf{U}}_T^k \to \mathbb{P}_d^k(T)$ is such that, for all $\underline{\mathsf{v}} = (\mathsf{v}_T, (\mathsf{v}_F)_{F\in\mathcal{F}_T}) \in \underline{\mathsf{U}}_T^k$ and all $q \in \mathbb{P}_d^k(T)$,

$$(D_T^k\underline{\mathsf{v}}, q)_T := -(\mathsf{v}_T, \nabla q)_T + \sum_{F\in\mathcal{F}_T} (\mathsf{v}_F\cdot\underline{n}_{TF}, q)_F \tag{23a}$$
$$= (\nabla\cdot\mathsf{v}_T, q)_T + \sum_{F\in\mathcal{F}_T} ((\mathsf{v}_F - \mathsf{v}_T)\cdot\underline{n}_{TF}, q)_F. \tag{23b}$$

A key point in our analysis is the following commuting diagram property.

Proposition 3 (Commuting property for discrete divergence operator). *Let $k \geqslant 0$ and let $T \in \mathcal{T}_h$. The following diagram commutes:*

$$\begin{array}{ccc} \underline{U}(T) & \xrightarrow{\nabla\cdot} & L^2(T) \\ {\scriptstyle I_T^k}\downarrow & & \downarrow{\scriptstyle \pi_T^k} \\ \underline{\mathsf{U}}_T^k & \xrightarrow{D_T^k} & \mathbb{P}_d^k(T) \end{array}$$

Proof. Let $T \in \mathcal{T}_h$, let $\underline{v} \in \underline{U}(T)$, and set $\underline{\mathsf{v}} := I_T^k \underline{v}$. We infer that, for all $q \in \mathbb{P}_d^k(T)$,

$$\begin{aligned} (\pi_T^k(\nabla\cdot\underline{v}), q)_T = (\nabla\cdot\underline{v}, q)_T &= -(\nabla q, \underline{v})_T + \sum_{F\in\mathcal{F}_T} (q, \underline{v}\cdot\underline{n}_{TF})_F \\ &= -(\nabla q, \pi_T^k\underline{v})_T + \sum_{F\in\mathcal{F}_T} (q, \pi_F^k\underline{v}\cdot\underline{n}_{TF})_F \\ &= -(\nabla q, \underline{\mathsf{v}}_T)_T + \sum_{F\in\mathcal{F}_T} (q, \underline{\mathsf{v}}_F\cdot\underline{n}_{TF})_F = (D_T^k\underline{\mathsf{v}}, q)_T, \end{aligned}$$

where we have used that $\nabla q \in \mathbb{P}_d^{k-1}(T)^d \subset \mathbb{P}_d^k(T)^d$, $q_{|F} \in \mathbb{P}_{d-1}^k(F)$, and (23a). □

4 Discrete problem and well-posedness

In this section we introduce the local and global bilinear forms, define the discrete problem, and establish its well-posedness. In what follows, we assume that $k \geqslant 1$.

4.1 Local bilinear forms

Let $T \in \mathcal{T}_h$. We define the local bilinear form on $\underline{\mathsf{U}}_T^k \times \underline{\mathsf{U}}_T^k$ such that, for all $\underline{\mathsf{v}}, \underline{\mathsf{w}} \in \underline{\mathsf{U}}_T^k$,

$$a_T(\underline{\mathsf{v}}, \underline{\mathsf{w}}) := 2\mu(\underline{\underline{E}}_T^k\underline{\mathsf{v}}, \underline{\underline{E}}_T^k\underline{\mathsf{w}})_T + \lambda(D_T^k\underline{\mathsf{v}}, D_T^k\underline{\mathsf{w}}) + (2\mu)s_T(\underline{\mathsf{v}}, \underline{\mathsf{w}}), \tag{24}$$

with stabilization bilinear form

$$s_T(\underline{\mathsf{v}}, \underline{\mathsf{w}}) := \sum_{F\in\mathcal{F}_T} h_F^{-1}(\pi_F^k(\underline{R}_T^k\underline{\mathsf{v}} - \underline{\mathsf{v}}_F), \pi_F^k(\underline{R}_T^k\underline{\mathsf{w}} - \underline{\mathsf{w}}_F))_F, \tag{25}$$

where, for $\underline{\mathsf{v}} = (\underline{\mathsf{v}}_T, (\underline{\mathsf{v}}_F)_{F\in\mathcal{F}_T}) \in \underline{\mathsf{U}}_T^k$, $\underline{R}_T^k\underline{\mathsf{v}} \in \mathbb{P}_d^{k+1}(T)^d$ is such that

$$\underline{R}_T^k\underline{\mathsf{v}} := \underline{\mathsf{v}}_T + (\underline{r}_T^k\underline{\mathsf{v}} - \pi_T^k\underline{r}_T^k\underline{\mathsf{v}}). \tag{26}$$

The term in parentheses can be interpreted as a higher-order correction of the element DOFs $\underline{\mathsf{v}}_T$ derived from the reconstructed field $\underline{r}_T^k\underline{\mathsf{v}}$ (note that this correction is independent of the closure relations in (15) for $k \geqslant 1$). The stabilization bilinear form s_T introduces a least-squares penalty of the L^2-orthogonal projection on $\mathbb{P}_{d-1}^k(F)^d$ of the difference between $\underline{\mathsf{v}}_F$ and $(\underline{R}_T^k\underline{\mathsf{v}})_{|F}$. This penalty is tailored to ensure stability, and, at the same time, to achieve the same convergence order as the symmetric gradient and divergence reconstruction operators in the error analysis. This important result is stated in the following lemma, where we introduce the following local discrete strain (semi-)norms on $\underline{\mathsf{U}}_T^k$: For all $\underline{\mathsf{v}} \in \underline{\mathsf{U}}_T^k$,

$$\|\underline{\mathsf{v}}\|_{\varepsilon,T}^2 := \|\nabla_{\mathrm{s}}\underline{\mathsf{v}}_T\|_T^2 + |\underline{\mathsf{v}}|_{\varepsilon,\partial T}^2, \qquad |\underline{\mathsf{v}}|_{\varepsilon,\partial T}^2 := \sum_{F\in\mathcal{F}_T} h_F^{-1}\|\underline{\mathsf{v}}_T - \underline{\mathsf{v}}_F\|_F^2. \tag{27}$$

Lemma 4 (Stabilization). *Assume $k \geqslant 1$. There is a real number $\eta > 0$ independent of h, μ, and λ such that, for all $T \in \mathcal{T}_h$ and all $\underline{\mathsf{v}} \in \underline{\mathsf{U}}_T^k$, the following stability property holds:*

$$\eta \|\underline{\mathsf{v}}\|_{\varepsilon,T}^2 \leqslant \|\underline{\underline{E}}_T^k \underline{\mathsf{v}}\|_T^2 + s_T(\underline{\mathsf{v}}, \underline{\mathsf{v}}) \leqslant \eta^{-1} \|\underline{\mathsf{v}}\|_{\varepsilon,T}^2. \tag{28}$$

Moreover, for all $\underline{v} \in H^{k+2}(T)^d$, the following approximation property holds:

$$s_T(I_T^k \underline{v}, I_T^k \underline{v})^{1/2} \lesssim h_T^{k+1} \|\underline{v}\|_{H^{k+2}(T)^d}. \tag{29}$$

Proof. (1) Let $T \in \mathcal{T}_h$ and let $\underline{\mathsf{v}} \in \underline{\mathsf{U}}_T^k$. We prove the first inequality in (28). Taking $\underline{w} = \underline{\mathsf{v}}_T$ in (17a), we infer that

$$\begin{aligned} \|\nabla_{\mathrm{s}} \underline{\mathsf{v}}_T\|_T^2 &= (\underline{\underline{E}}_T^k \underline{\mathsf{v}}, \nabla_{\mathrm{s}} \underline{\mathsf{v}}_T)_T + \sum_{F \in \mathcal{F}_T} (\underline{\mathsf{v}}_T - \underline{\mathsf{v}}_F, \nabla_{\mathrm{s}} \underline{\mathsf{v}}_T \underline{n}_{TF})_F \\ &\leqslant \|\underline{\underline{E}}_T^k \underline{\mathsf{v}}\|_T^2 + \frac{1}{2} \|\nabla_{\mathrm{s}} \underline{\mathsf{v}}_T\|_T^2 + N_\partial C_{\mathrm{tr}}^2 |\underline{\mathsf{v}}|_{\varepsilon,\partial T}^2, \end{aligned} \tag{30}$$

where we have used the Cauchy–Schwarz and Young inequalities followed by the discrete trace inequality (5) for the last term on the right-hand side. As a result,

$$\|\nabla_{\mathrm{s}} \underline{\mathsf{v}}_T\|_T^2 \lesssim \|\underline{\underline{E}}_T^k \underline{\mathsf{v}}\|_T^2 + |\underline{\mathsf{v}}|_{\varepsilon,\partial T}^2. \tag{31}$$

Additionally, for all $F \in \mathcal{F}_T$,

$$\begin{aligned} h_F^{-1/2} \|\underline{\mathsf{v}}_F - \underline{\mathsf{v}}_T\|_F &\leqslant h_F^{-1/2} \|\underline{\mathsf{v}}_F - \pi_F^k \underline{R}_T^k \underline{\mathsf{v}}\|_F + h_F^{-1/2} \|\pi_F^k \underline{R}_T^k \underline{\mathsf{v}} - \underline{\mathsf{v}}_T\|_F \\ &= h_F^{-1/2} \|\pi_F^k (\underline{\mathsf{v}}_F - \underline{R}_T^k \underline{\mathsf{v}})\|_F + h_F^{-1/2} \|\pi_F^k (\underline{R}_T^k \underline{\mathsf{v}} - \underline{\mathsf{v}}_T)\|_F \\ &= h_F^{-1/2} \|\pi_F^k (\underline{\mathsf{v}}_F - \underline{R}_T^k \underline{\mathsf{v}})\|_F + C_{\mathrm{tr}} h_F^{-1} \|\underline{r}_T^k \underline{\mathsf{v}} - \pi_T^k \underline{r}_T^k \underline{\mathsf{v}}\|_T \end{aligned} \tag{32}$$

where we have used the triangle inequality in the first line, the fact that $\underline{\mathsf{v}}_F \in \mathbb{P}_{d-1}^k(F)^d$ and $\underline{\mathsf{v}}_{T|F} \in \mathbb{P}_{d-1}^k(F)^d$ in the second line, and the fact that π_F^k is a projector, the definition (26) of $\underline{R}_T^k$, and the discrete trace inequality (5) in the third line. For any function $\underline{w} \in H^1(T)^d$, writing $\underline{w}_{\mathrm{RM}} = |T|_d^{-1} (\int_T \underline{w}) + |T|_d^{-1} (\int_T \nabla_{\mathrm{ss}} \underline{w})(\underline{x} - \underline{x}_T)$, where $\underline{x}_T$ denotes the barycenter of T, we observe that $\pi_T^k \underline{w}_{\mathrm{RM}} = \underline{w}_{\mathrm{RM}}$ since $k \geqslant 1$, whence we infer that

$$\|\underline{w} - \pi_T^k \underline{w}\|_T = \|(\underline{w} - \underline{w}_{\mathrm{RM}}) - \pi_T^k (\underline{w} - \underline{w}_{\mathrm{RM}})\|_T \leqslant \|\underline{w} - \underline{w}_{\mathrm{RM}}\|_T \lesssim h_T \|\nabla_{\mathrm{s}} \underline{w}\|_T,$$

where we have used the fact that π_T^k is an L^2-projector and Korn's inequality (11) since $(\underline{w} - \underline{w}_{\mathrm{RM}}) \in \underline{\mathcal{U}}(T)$. Applying this bound to $\underline{w} = \underline{r}_T^k \underline{\mathsf{v}}$, using the mesh regularity property (3), and recalling the definition (14) of $\underline{r}_T^k$, the last term on the right-hand side of (32) can be estimated as

$$C_{\mathrm{tr}} h_F^{-1} \|\underline{r}_T^k \underline{\mathsf{v}} - \pi_T^k \underline{r}_T^k \underline{\mathsf{v}}\|_T \leqslant \varrho^{-2} C_{\mathrm{tr}} C_{\mathrm{K}} \|\underline{\underline{E}}_T^k \underline{\mathsf{v}}\|_T,$$

so that

$$h_F^{-1/2} \|\underline{\mathsf{v}}_F - \underline{\mathsf{v}}_T\|_F \lesssim h_F^{-1/2} \|\pi_F^k (\underline{\mathsf{v}}_F - \underline{R}_T^k \underline{\mathsf{v}})\|_F + \|\underline{\underline{E}}_T^k \underline{\mathsf{v}}\|_T. \tag{33}$$

Squaring (33), summing over $F \in \mathcal{F}_T$, and using the bound (4) on $\mathrm{card}(\mathcal{F}_T)$ leads to

$$|\underline{\mathsf{v}}|_{\varepsilon,\partial T}^2 \lesssim s_T(\underline{\mathsf{v}}, \underline{\mathsf{v}}) + \|\underline{\underline{E}}_T^k \underline{\mathsf{v}}\|_T^2. \tag{34}$$

The first inequality in (28) immediately follows from (31) and (34). The proof of the second inequality in (28) uses similar arguments and is omitted for the sake of brevity.

(2) Let us now prove (29) for all $\underline{v} \in H^{k+2}(T)^d$. We observe that, for all $T \in \mathcal{T}_h$ and all $F \in \mathcal{F}_T$,

$$\begin{aligned} h_F^{-1/2}\|\pi_F^k(\underline{R}_T^k I_T^k \underline{v} - \pi_F^k \underline{v})\|_F &\leqslant h_F^{-1/2}\|\underline{R}_T^k I_T^k \underline{v} - \underline{v}\|_F \\ &= h_F^{-1/2}\|(\underline{r}_T^k I_T^k \underline{v} - \underline{v}) - \pi_T^k(\underline{r}_T^k I_T^k \underline{v} - \underline{v})\|_F \\ &\lesssim h_F^{-1/2}\|\underline{r}_T^k I_T^k \underline{v} - \underline{v}\|_F + C_{\mathrm{tr}} h_F^{-1}\|\underline{r}_T^k I_T^k \underline{v} - \underline{v}\|_T \\ &\lesssim h_T^{k+1}\|\underline{v}\|_{H^{k+2}(T)^d}, \end{aligned} \tag{35}$$

where we have used the fact that π_F^k is a projector and the definition of the faces DOFs of $I_T^k \underline{v}$ in the first line, the definition (26) of $\underline{R}_T^k$ in the second line, the triangle inequality, the discrete trace inequality (5), and the fact that π_T^k is a projector in the third line, and the approximation property (18) of $\underline{r}_T^k I_T^k$ and the mesh regularity property (3) in the fourth line. Recalling the definition (25) of s_T, the bound (29) readily follows from (35) and the bound (4) on $\mathrm{card}(\mathcal{F}_T)$. □

4.2 Global bilinear forms

Going from local to global bilinear forms proceeds, as in standard finite element methods, by a cell-wise assembly. The global space of DOFs is obtained by patching local DOFs at interfaces, yielding

$$\underline{\mathsf{U}}_h^k := \left\{ \bigtimes_{T\in\mathcal{T}_h} \mathbb{P}_d^k(T)^d \right\} \times \left\{ \bigtimes_{F\in\mathcal{F}_h} \mathbb{P}_{d-1}^k(F)^d \right\}. \tag{36}$$

For $\underline{\mathsf{v}}_h \in \underline{\mathsf{U}}_h^k$, we use the notation $\underline{\mathsf{v}}_h = ((\underline{\mathsf{v}}_T)_{T\in\mathcal{T}_h}, (\underline{\mathsf{v}}_F)_{F\in\mathcal{F}_h})$. For all $T \in \mathcal{T}_h$, we denote by L_T the restriction operator that maps the global DOFs in $\underline{\mathsf{U}}_h^k$ to the corresponding local DOFs in $\underline{\mathsf{U}}_T^k$, i.e., for all $\underline{\mathsf{v}}_h \in \underline{\mathsf{U}}_h^k$, $\mathsf{L}_T\underline{\mathsf{v}}_h = (\underline{\mathsf{v}}_T, (\underline{\mathsf{v}}_F)_{F\in\mathcal{F}_T}) \in \underline{\mathsf{U}}_T^k$. The homogeneous Dirichlet boundary condition on the displacement can be enforced explicitly on the DOFs attached to boundary faces. We set

$$\underline{\mathsf{U}}_{h,0}^k := \left\{ \underline{\mathsf{v}}_h = ((\underline{\mathsf{v}}_T)_{T\in\mathcal{T}_h}, (\underline{\mathsf{v}}_F)_{F\in\mathcal{F}_h}) \in \underline{\mathsf{U}}_h^k \mid \underline{\mathsf{v}}_F \equiv \underline{0}\ \forall F \in \mathcal{F}_h^{\mathrm{b}} \right\}, \tag{37}$$

The global bilinear forms a_h and s_h are assembled cell-wise as follows: For all $\underline{\mathsf{v}}_h, \underline{\mathsf{w}}_h \in \underline{\mathsf{U}}_h^k$,

$$a_h(\underline{\mathsf{v}}_h, \underline{\mathsf{w}}_h) := \sum_{T\in\mathcal{T}_h} a_T(\mathsf{L}_T\underline{\mathsf{v}}_h, \mathsf{L}_T\underline{\mathsf{w}}_h), \qquad s_h(\underline{\mathsf{v}}_h, \underline{\mathsf{w}}_h) := \sum_{T\in\mathcal{T}_h} s_T(\mathsf{L}_T\underline{\mathsf{v}}_h, \mathsf{L}_T\underline{\mathsf{w}}_h). \tag{38}$$

The loading term is discretized by means of the linear form l_h on $\underline{\mathsf{U}}_h^k$ such that, for all $\underline{\mathsf{v}}_h \in \underline{\mathsf{U}}_h^k$,

$$l_h(\underline{\mathsf{v}}_h) := \sum_{T\in\mathcal{T}_h} \int_T \underline{f}\cdot\underline{\mathsf{v}}_T. \tag{39}$$

The discrete problem reads: Find $\underline{\mathsf{u}}_h \in \underline{\mathsf{U}}_{h,0}^k$ such that, for all $\underline{\mathsf{v}}_h \in \underline{\mathsf{U}}_{h,0}^k$,

$$a_h(\underline{\mathsf{u}}_h, \underline{\mathsf{v}}_h) = l_h(\underline{\mathsf{v}}_h). \tag{40}$$

The global strain (semi-)norm is such that, for all $\underline{\mathsf{v}}_h \in \underline{\mathsf{U}}_h^k$,

$$\|\underline{\mathsf{v}}_h\|_{\varepsilon,h}^2 := \sum_{T\in\mathcal{T}_h} \|\mathsf{L}_T\underline{\mathsf{v}}_h\|_{\varepsilon,T}^2. \tag{41}$$

Proposition 5 (Norm $\|\cdot\|_{\varepsilon,h}$). *The map $\|\cdot\|_{\varepsilon,h}$ defined by (41) is a norm on $\underline{\mathbf{U}}_{h,0}^k$.*

Proof. It suffices to show that, for all $\underline{\mathbf{v}}_h \in \underline{\mathbf{U}}_{h,0}^k$, $\|\underline{\mathbf{v}}_h\|_{\varepsilon,h} = 0$ if and only if $\underline{\mathbf{v}}_T \equiv \underline{0}$ for all $T \in \mathcal{T}_h$ and $\underline{\mathbf{v}}_F \equiv \underline{0}$ for all $F \in \mathcal{F}_h$. We start by observing that $\|\underline{\mathbf{v}}_h\|_{\varepsilon,h} = 0$ means that

$$\forall T \in \mathcal{T}_h, \qquad \nabla_{\mathrm{s}}\underline{\mathbf{v}}_T \equiv \underline{\underline{0}} \quad \text{and} \quad \underline{\mathbf{v}}_T - \underline{\mathbf{v}}_F \equiv \underline{0} \quad \forall F \in \mathcal{F}_h.$$

For a boundary element $T \in \mathcal{T}_h$ with $F \in \mathcal{F}_T \cap \mathcal{F}_h^{\mathrm{b}}$, using $\underline{\mathbf{v}}_F \equiv \underline{0}$ (cf. the definition (37) of $\underline{\mathbf{U}}_{h,0}^k$), we infer that $\underline{\mathbf{v}}_{T|F} \equiv \underline{0}$ which, combined with $\nabla_{\mathrm{s}}\underline{\mathbf{v}}_T \equiv \underline{\underline{0}}$ and Korn's inequality, implies $\underline{\mathbf{v}}_T \equiv \underline{0}$ and, hence, $\underline{\mathbf{v}}_{F'} \equiv \underline{0}$ for all $F' \in \mathcal{F}_T \backslash \{F\}$ since $\underline{\mathbf{v}}_T - \underline{\mathbf{v}}_{F'} \equiv \underline{0}$. Repeating the argument for the next layer of elements (and the corresponding faces), the result is proved iterating until all elements and faces have been visited. □

Corollary 6 (Well-posedness of (40)). *Assume $k \geqslant 1$. For all $\underline{\mathbf{v}}_h \in \underline{\mathbf{U}}_h^k$, the following inequality holds:*

$$\eta\|\underline{\mathbf{v}}_h\|_{\varepsilon,h}^2 \leqslant \sum_{T\in\mathcal{T}_h} \left\{ \|\underline{\underline{E}}_T^k \mathsf{L}_T\underline{\mathbf{v}}_h\|_T^2 + s_T(\mathsf{L}_T\underline{\mathbf{v}}_h, \mathsf{L}_T\underline{\mathbf{v}}_h) \right\} \leqslant \eta^{-1}\|\underline{\mathbf{v}}_h\|_{\varepsilon,h}^2, \tag{42}$$

with η resulting from Lemma 4. As a consequence, problem (40) is well-posed.

Proof. Inequalities (42) follow from (28) by summing over $T \in \mathcal{T}_h$. The well-posedness of (40) then follows from the Lax–Milgram Lemma and Proposition 5. □

Remark 7 (Bound on $\|\cdot\|$-norm). *Using discrete Korn inequalities for piecewise smooth fields, see Duarte et al. [17] and Brenner [7], and a triangle inequality for the face term, we infer the following stronger result on the $\|\cdot\|_{\varepsilon,h}$-norm: For all $\underline{\mathbf{v}}_h \in \underline{\mathbf{U}}_{h,0}^k$, $\|\underline{\mathbf{v}}_h\|_{\varepsilon,h} \gtrsim C\|\underline{v}_h\|$ with real number $C > 0$ independent of h and $\underline{v}_h$ reconstructed from the element-based DOFs of $\underline{\mathbf{v}}_h$ as $(\underline{v}_h)_{|T} = \underline{\mathbf{v}}_T$ for all $T \in \mathcal{T}_h$.*

5 Error analysis

5.1 Basic error estimate

Let $\underline{u} \in \underline{U}_0$ and $\underline{\mathbf{u}}_h \in \underline{\mathbf{U}}_{h,0}^k$ denote the unique solutions to (2) and (40), respectively. We bound the error $\underline{\mathbf{u}}_h - \widehat{\underline{\mathbf{u}}}_h$, where $\widehat{\underline{\mathbf{u}}}_h \in \underline{\mathbf{U}}_{h,0}^k$ is such that $\widehat{\underline{\mathbf{u}}}_h = ((\pi_T^k\underline{u})_{T\in\mathcal{T}_h}, (\pi_F^k\underline{u})_{F\in\mathcal{F}_h})$. Observe that $\widehat{\underline{\mathbf{u}}}_h$ is obtained from the exact solution $\underline{u}$ using the local reduction maps on each mesh element, i.e., $\mathsf{L}_T\widehat{\underline{\mathbf{u}}}_h = I_T^k(\underline{u}_{|T})$. We measure the error in the energy norm such that, for all $\underline{\mathbf{v}}_h \in \underline{\mathbf{U}}_h^k$,

$$\|\underline{\mathbf{v}}_h\|_{\mathrm{en},h}^2 := a_h(\underline{\mathbf{v}}_h, \underline{\mathbf{v}}_h). \tag{43}$$

Owing to the lower bound in (42), we observe that $\|\underline{\mathbf{v}}_h\|_{\mathrm{en},h}^2 \geqslant (2\mu\eta)\|\underline{\mathbf{v}}_h\|_{\varepsilon,h}^2$. In what follows, we formulate the regularity of the exact solution using broken (piecewise) Sobolev spaces $H^m(\mathcal{T}_h)$ for some positive integer m equipped with the norm $\|\cdot\|_{H^m(\mathcal{T}_h)}^2 = \sum_{T\in\mathcal{T}_h}\|\cdot\|_{H^m(T)}^2$.

Theorem 8 (Convergence). *Assume $k \geqslant 1$ and the additional regularity $\underline{u} \in H^{k+2}(\mathcal{T}_h)^d$ and $\nabla\cdot\underline{u} \in H^{k+1}(\mathcal{T}_h)$. Then, there exists a real number $C > 0$ independent of h, μ, and λ, such that*

$$(2\mu)^{1/2}\|\underline{\mathbf{u}}_h - \widehat{\underline{\mathbf{u}}}_h\|_{\mathrm{en},h} \leqslant Ch^{k+1}\left(2\mu\|\underline{u}\|_{H^{k+2}(\mathcal{T}_h)^d} + \lambda\|\nabla\cdot\underline{u}\|_{H^{k+1}(\mathcal{T}_h)}\right). \tag{44}$$

Remark 9 (Locking-free estimate). *For $d = 2$ and Ω convex, it is proven in [8] that*

$$\mu\|\underline{u}\|_{H^2(\Omega)^d} + \lambda\|\nabla{\cdot}\underline{u}\|_{H^1(\Omega)} \leqslant C_\mu\|\underline{f}\|, \tag{45}$$

where $C_\mu > 0$ denotes a real number depending on Ω and μ but independent of λ. More generally, for $k \geqslant 1$, we need the regularity shift $\mu\|\underline{u}\|_{H^{k+2}(\Omega)^d} + \lambda\|\nabla{\cdot}\underline{u}\|_{H^{k+1}(\Omega)} \leqslant C_\mu\|\underline{f}\|_{H^k(\Omega)^d}$.

Proof. For all $\underline{\mathsf{v}}_h \in \underline{\mathsf{U}}_{h,0}^k$, we observe that

$$\|\underline{\mathsf{v}}_h\|_{\mathrm{en},h}^2 = a_h(\underline{\mathsf{v}}_h, \underline{\mathsf{v}}_h) \leqslant \left\{ \sup_{\underline{\mathsf{w}}_h \in \underline{\mathsf{U}}_{h,0}^k} \frac{a_h(\underline{\mathsf{v}}_h, \underline{\mathsf{w}}_h)}{\|\underline{\mathsf{w}}_h\|_{\varepsilon,h}} \right\} \times \|\underline{\mathsf{v}}_h\|_{\varepsilon,h}.$$

Since $\|\underline{\mathsf{v}}_h\|_{\mathrm{en},h} \geqslant (2\mu\eta)^{1/2}\|\underline{\mathsf{v}}_h\|_{\varepsilon,h}$, we infer that

$$(2\mu\eta)^{1/2}\|\underline{\mathsf{v}}_h\|_{\mathrm{en},h} \leqslant \sup_{\underline{\mathsf{w}}_h \in \underline{\mathsf{U}}_{h,0}^k, \|\underline{\mathsf{w}}_h\|_{\varepsilon,h}=1} a_h(\underline{\mathsf{v}}_h, \underline{\mathsf{w}}_h).$$

Applying this inequality to the error $(\underline{\mathsf{u}}_h - \widehat{\underline{\mathsf{u}}}_h)$ and using (40) yields

$$(2\mu\eta)^{1/2}\|\underline{\mathsf{u}}_h - \widehat{\underline{\mathsf{u}}}_h\|_{\mathrm{en},h} \leqslant \sup_{\underline{\mathsf{v}}_h \in \underline{\mathsf{U}}_{h,0}^k, \|\underline{\mathsf{w}}_h\|_{\varepsilon,h}=1} \mathcal{E}_h(\underline{\mathsf{w}}_h), \tag{46}$$

with consistency error $\mathcal{E}_h(\underline{\mathsf{w}}_h) := l_h(\underline{\mathsf{w}}_h) - a_h(\widehat{\underline{\mathsf{u}}}_h, \underline{\mathsf{w}}_h)$. We bound $\mathcal{E}_h(\underline{\mathsf{w}}_h)$ for a generic $\underline{\mathsf{w}}_h \in \underline{\mathsf{U}}_{h,0}^k$ such that $\|\underline{\mathsf{w}}_h\|_{\varepsilon,h} = 1$. Recalling that $\underline{f} = -\nabla{\cdot}\underline{\sigma}$ a.e. in Ω, and integrating by parts elementwise, we infer that

$$l_h(\underline{\mathsf{w}}_h) = \sum_{T\in\mathcal{T}_h} \left\{ 2\mu(\nabla_{\mathrm{s}}\underline{u}, \nabla_{\mathrm{s}}\underline{\mathsf{w}}_T)_T + \lambda(\nabla{\cdot}\underline{u}, \nabla{\cdot}\underline{\mathsf{w}}_T)_T - \sum_{F\in\mathcal{F}_T} (\underline{\sigma}\underline{n}_{TF}, \underline{\mathsf{w}}_T - \underline{\mathsf{w}}_F)_F \right\}, \tag{47}$$

where we have used the continuity of the normal stress component at interfaces together with $\underline{\mathsf{w}}_F \equiv \underline{0}$ for all $F \in \mathcal{F}_h^{\mathrm{b}}$ to infer that $\sum_{T\in\mathcal{T}_h}\sum_{F\in\mathcal{F}_T}(\underline{\sigma}\underline{n}_{TF}, \underline{\mathsf{w}}_F)_F = 0$. Taking $\underline{w} = \breve{\underline{u}}_T := \underline{r}_T^k\mathsf{L}_T\widehat{\underline{\mathsf{u}}}_h = \underline{r}_T^k I_T^k(\underline{u}_{|T})$ in the definition (17a) of $\underline{\underline{E}}_T^k\mathsf{L}_T\underline{\mathsf{w}}_h$ for all $T \in \mathcal{T}_h$, we infer that

$$(\underline{\underline{E}}_T^k\mathsf{L}_T\widehat{\underline{\mathsf{u}}}_h, \underline{\underline{E}}_T^k\mathsf{L}_T\underline{\mathsf{w}}_h)_T = (\nabla_{\mathrm{s}}\breve{\underline{u}}_T, \nabla_{\mathrm{s}}\underline{\mathsf{w}}_T)_T + \sum_{F\in\mathcal{F}_T} (\nabla_{\mathrm{s}}\breve{\underline{u}}_T\underline{n}_{TF}, \underline{\mathsf{w}}_F - \underline{\mathsf{w}}_T)_F. \tag{48}$$

Similarly, taking $q := \pi_T^k(\nabla{\cdot}\underline{u})$ in the definition (23b) of $D_T^k\mathsf{L}_T\underline{\mathsf{w}}_h$ for all $T \in \mathcal{T}_h$, and recalling the local commuting diagram property for I_T^k, we infer that

$$\begin{aligned}(D_T^k\mathsf{L}_T\widehat{\underline{\mathsf{u}}}_h, D_T^k\mathsf{L}_T\underline{\mathsf{w}}_h)_T &= (\pi_T^k(\nabla{\cdot}\underline{u}), D_T^k\mathsf{L}_T\underline{\mathsf{w}}_h)_T \\ &= (\nabla{\cdot}\underline{u}, \nabla{\cdot}\underline{\mathsf{w}}_T)_T + \sum_{F\in\mathcal{F}_T} (\pi_T^k(\nabla{\cdot}\underline{u}), (\underline{\mathsf{w}}_F - \underline{\mathsf{w}}_T){\cdot}\underline{n}_{TF})_F,\end{aligned} \tag{49}$$

since $\nabla{\cdot}\underline{\mathsf{w}}_T \in \mathbb{P}_d^{k-1}(T) \subset \mathbb{P}_d^k(T)$. Using (47)–(49) to replace the corresponding terms in the expression of $\mathcal{E}_h(\underline{\mathsf{w}}_h)$, we infer that

$$\begin{aligned}\mathcal{E}_h(\underline{\mathsf{w}}_h) = &\sum_{T\in\mathcal{T}_h} 2\mu \left\{ (\nabla_{\mathrm{s}}(\underline{u} - \breve{\underline{u}}_T), \nabla_{\mathrm{s}}\underline{\mathsf{w}}_T)_T + \sum_{F\in\mathcal{F}_T} (\nabla_{\mathrm{s}}(\underline{u} - \breve{\underline{u}}_T)\underline{n}_{TF}, \underline{\mathsf{w}}_F - \underline{\mathsf{w}}_T)_F \right\} \\ &- \sum_{F\in\mathcal{F}_T} \lambda((\nabla{\cdot}\underline{u} - \pi_T^k(\nabla{\cdot}\underline{u}))\underline{n}_{TF}, \underline{\mathsf{w}}_T - \underline{\mathsf{w}}_F)_F - (2\mu)s_h(\widehat{\underline{\mathsf{u}}}_h, \underline{\mathsf{w}}_h) := \mathfrak{T}_1 + \mathfrak{T}_2 + \mathfrak{T}_3.\end{aligned} \tag{50}$$

To estimate $\mathfrak{T}_1$, we use the Cauchy–Schwarz inequality, the approximation property (18) of $\underline{r}_T^k I_T^k$, and the mesh regularity properties (3) and (4) to infer that

$$|\mathfrak{T}_1| \lesssim 2\mu h^{k+1} \|\underline{u}\|_{H^{k+2}(\mathcal{T}_h)^d} \|\underline{\mathsf{w}}_h\|_{\varepsilon,h}. \tag{51}$$

Proceeding similarly for $\mathfrak{T}_2$ using the approximation property (7) of π_T^k yields

$$|\mathfrak{T}_2| \lesssim \lambda h^{k+1} \|\nabla{\cdot}\underline{u}\|_{H^{k+1}(\mathcal{T}_h)} \|\underline{\mathsf{w}}_h\|_{\varepsilon,h}. \tag{52}$$

To estimate $\mathfrak{T}_3$, we infer from the symmetry and positivity of s_h that

$$|\mathfrak{T}_3| \leqslant (2\mu) s_h(\widehat{\underline{\mathsf{u}}}_h, \widehat{\underline{\mathsf{u}}}_h)^{1/2} s_h(\underline{\mathsf{w}}_h, \underline{\mathsf{w}}_h)^{1/2} \lesssim 2\mu h^{k+1} \|\underline{u}\|_{H^{k+2}(\mathcal{T}_h)^d} \|\underline{\mathsf{w}}_h\|_{\varepsilon,h}, \tag{53}$$

where we have used (29) to estimate the first factor and the second bound in (28) to estimate the second factor. The bound (44) follows using inequalities (51), (52), and (53) to estimate the right-hand side of (50), and using the resulting bound in (46). □

We now infer an energy error estimate comparing $\nabla_{\mathrm{s}}\underline{u}$ to the global (nonconforming) symmetric gradient reconstruction $\underline{\underline{E}}_h^k \underline{\mathsf{u}}_h$ such that $\underline{\underline{E}}_h^k \underline{\mathsf{u}}_{h|T} = \underline{\underline{E}}_T^k \mathsf{L}_T \underline{\mathsf{u}}_h$ for all $T \in \mathcal{T}_h$.

Corollary 10 (Estimate on symmetric gradient reconstruction)**.** *Under the assumptions of Theorem 8, the following holds:*

$$(2\mu)\|\nabla_{\mathrm{s}}\underline{u} - \underline{\underline{E}}_h^k \underline{\mathsf{u}}_h\| \leqslant C h^{k+1} \left(2\mu \|\underline{u}\|_{H^{k+2}(\mathcal{T}_h)^d} + \lambda \|\nabla{\cdot}\underline{u}\|_{H^{k+1}(\mathcal{T}_h)} \right), \tag{54}$$

where $C > 0$ is a real number independent of h, μ, and λ.

Proof. For all $T \in \mathcal{T}_h$, the triangle inequality yields

$$\|\nabla_{\mathrm{s}}\underline{u} - \underline{\underline{E}}_T^k \mathsf{L}_T \underline{\mathsf{u}}_h\|_T \leqslant \|\nabla_{\mathrm{s}}(\underline{u} - \underline{r}_T^k I_T^k \underline{u})\|_T + \|\underline{\underline{E}}_T^k \mathsf{L}_T (\widehat{\underline{\mathsf{u}}}_h - \underline{\mathsf{u}}_h)\|_T,$$

since $\nabla_{\mathrm{s}}(\underline{r}_T^k I_T^k \underline{u})_{|T} = \underline{\underline{E}}_T^k \mathsf{L}_T \widehat{\underline{\mathsf{u}}}_h$. The first term on the right-hand side is bounded using Lemma 2 and the second one using Theorem 8. □

5.2 L^2-error estimate for the displacement

In this section, we bound the $\|\cdot\|$-norm of the displacement error. We assume elliptic regularity in the following form: For all $\underline{g} \in L^2(\Omega)^d$, the unique solution of

$$\begin{aligned} -\nabla{\cdot}\underline{\underline{\varsigma}} &= \underline{g} && \text{in } \Omega, \\ \underline{\underline{\varsigma}} &= 2\mu \nabla_{\mathrm{s}}\underline{z} + \lambda(\nabla{\cdot}\underline{z})\underline{\underline{I}}_d && \text{in } \Omega, \\ \underline{z} &= 0 && \text{on } \partial\Omega, \end{aligned} \tag{55}$$

satisfies the a priori estimate

$$\mu \|\underline{z}\|_{H^2(\Omega)^d} + \lambda \|\nabla{\cdot}\underline{z}\|_{H^1(\Omega)} \leqslant C_\mu \|\underline{g}\|. \tag{56}$$

We first consider the displacement error $\underline{e}_h$ such that $\underline{e}_{h|T} := \underline{\mathsf{u}}_T - \pi_T^k \underline{u} \in \mathbb{P}_d^k(T)^d$ for all $T \in \mathcal{T}_h$.

Theorem 11 (L^2-error estimate for the displacement)**.** *Under the assumptions of Theorem 8 and the elliptic regularity assumption* (56)*, the following holds:*

$$\|\underline{e}_h\| \leqslant Ch^{k+2}\left(2\mu\|\underline{u}\|_{H^{k+2}(\mathcal{T}_h)^d} + \lambda\|\nabla{\cdot}\underline{u}\|_{H^{k+1}(\mathcal{T}_h)}\right), \tag{57}$$

where $C>0$ is a real number depending on Ω, μ, and ϱ, but independent of λ and h.

Proof. In the proof, we abbreviate by $a \lesssim b$ the inequality $a \leqslant Cb$ with real number $C>0$ independent of h and λ, but possibly depending on μ. Since $\|{\cdot}\|_{\mathrm{en},h} \geqslant (2\mu\eta)^{1/2}\|{\cdot}\|_{\varepsilon,h}$ and $\|{\cdot}\|_{\mathrm{en},h} \geqslant (2\mu)s_h({\cdot},{\cdot})^{1/2}$, we infer from the error estimate (44) that, with $\underline{\mathsf{e}}_h := \underline{\mathsf{u}}_h - \widehat{\underline{\mathsf{u}}}_h \in \underline{\mathsf{U}}_{h,0}^k$ and $B(\underline{u},k) := 2\mu\|\underline{u}\|_{H^{k+2}(\mathcal{T}_h)^d} + \lambda\|\nabla{\cdot}\underline{u}\|_{H^{k+1}(\mathcal{T}_h)}$,

$$\|\underline{\mathsf{e}}_h\|_{\varepsilon,h} + s_h(\underline{\mathsf{e}}_h,\underline{\mathsf{e}}_h)^{1/2} \lesssim h^{k+1}B(\underline{u},k). \tag{58}$$

Consider the auxiliary problem (55) with $\underline{g} := \underline{e}_h$ and corresponding solution $\underline{z}$ and $\underline{\underline{\varsigma}}$. Integrating by parts element-wise and since $\underline{e}_{h|T} = \underline{\mathsf{e}}_T$, we infer that

$$\|\underline{e}_h\|^2 = -\sum_{T\in\mathcal{T}_h}(\underline{\mathsf{e}}_T,\nabla{\cdot}\underline{\underline{\varsigma}})_T = \sum_{T\in\mathcal{T}_h}\left\{(\nabla_{\mathrm{s}}\underline{\mathsf{e}}_T,\underline{\underline{\varsigma}})_T + \sum_{F\in\mathcal{F}_T}(\underline{\mathsf{e}}_F-\underline{\mathsf{e}}_T,\underline{\underline{\varsigma}}\underline{n}_{TF})_F\right\}, \tag{59}$$

where we have used the continuity of the normal component of $\underline{\underline{\varsigma}}$ across interfaces together with the fact that $\underline{\mathsf{e}}_F \equiv \underline{0}$ for all $F\in\mathcal{F}_h^{\mathrm{b}}$. Let $\widehat{\underline{\mathsf{z}}}_h := ((\pi_T^k\underline{z})_{T\in\mathcal{T}_h},(\pi_F^k\underline{z})_{F\in\mathcal{F}_h}) \in \underline{\mathsf{U}}_{h,0}^k$ (so that $\mathsf{L}_T\widehat{\underline{\mathsf{z}}}_h = I_T^k\underline{z}_{|T}$) and observe that, for all $T\in\mathcal{T}_h$,

$$\|\nabla_{\mathrm{s}}(\underline{z}-\underline{r}_T^kI_T^k\underline{z})\|_T + h_T^{1/2}\|\nabla_{\mathrm{s}}(\underline{z}-\underline{r}_T^kI_T^k\underline{z})\|_{\partial T} \lesssim h_T\|\underline{z}\|_{H^2(T)^d}, \tag{60a}$$

$$\|\nabla{\cdot}\underline{z}-\pi_T^k(\nabla{\cdot}\underline{z})\|_T + h_T^{1/2}\|\nabla{\cdot}\underline{z}-\pi_T^k(\nabla{\cdot}\underline{z})\|_{\partial T} \lesssim h_T\|\nabla{\cdot}\underline{z}\|_{H^1(T)}, \tag{60b}$$

$$s_T(I_T^k\underline{z},I_T^k\underline{z})^{1/2} \lesssim h_T\|\underline{z}\|_{H^2(T)^d}. \tag{60c}$$

Estimate (60a) is proved as in Lemma 2; estimate (60b) results from the approximation properties (7) of π_T^k; estimate (60c) is proved as in Lemma 4. Since $a_h(\underline{\mathsf{e}}_h,\widehat{\underline{\mathsf{z}}}_h) = \mathcal{E}_h(\widehat{\underline{\mathsf{z}}}_h)$ with $\mathcal{E}_h(\widehat{\underline{\mathsf{z}}}_h) = l_h(\widehat{\underline{\mathsf{z}}}_h) - a_h(\widehat{\underline{\mathsf{u}}}_h,\widehat{\underline{\mathsf{z}}}_h)$, we rewrite (59) as follows:

$$\|\underline{e}_h\|^2 = \left\{\sum_{T\in\mathcal{T}_h}\left[(\nabla_{\mathrm{s}}\underline{\mathsf{e}}_T,\underline{\underline{\varsigma}})_T + \sum_{F\in\mathcal{F}_T}(\underline{\mathsf{e}}_F-\underline{\mathsf{e}}_T,\underline{\underline{\varsigma}}\underline{n}_{TF})_F\right] - a_h(\underline{\mathsf{e}}_h,\widehat{\underline{\mathsf{z}}}_h)\right\} + \mathcal{E}_h(\widehat{\underline{\mathsf{z}}}_h) := \mathfrak{T}_1+\mathfrak{T}_2. \tag{61}$$

For all $T\in\mathcal{T}_h$, using the definition (17a) of $\underline{\underline{E}}_T^k\mathsf{L}_T\underline{\mathsf{e}}_h$ with $\underline{w} = \underline{r}_T^k\mathsf{L}_T\widehat{\underline{\mathsf{z}}}_h$ and the definition (23b) of $D_T^k\mathsf{L}_T\underline{\mathsf{e}}_h$ with $q = D_T^k\mathsf{L}_T\widehat{\underline{\mathsf{z}}}_h$, we infer that

$$a_h(\underline{\mathsf{e}}_h,\widehat{\underline{\mathsf{z}}}_h) = \sum_{T\in\mathcal{T}_h}\left\{(\nabla_{\mathrm{s}}\underline{\mathsf{e}}_T,\underline{\underline{S}}_T^k)_T + \sum_{F\in\mathcal{F}_T}(\underline{\mathsf{e}}_F-\underline{\mathsf{e}}_T,\underline{\underline{S}}_T^k\underline{n}_{TF})_F\right\} + (2\mu)s_h(\underline{\mathsf{e}}_h,\widehat{\underline{\mathsf{z}}}_h), \tag{62}$$

with $\underline{\underline{S}}_T^k := 2\mu\underline{\underline{E}}_T^k\mathsf{L}_T\widehat{\underline{\mathsf{z}}}_h + \lambda(D_T^k\mathsf{L}_T\widehat{\underline{\mathsf{z}}}_h)\underline{\underline{I}}_d$. Plugging this expression into $\mathfrak{T}_1$, multiple uses of the Cauchy–Schwarz inequality together with the fact that $s_h(\underline{\mathsf{e}}_h,\widehat{\underline{\mathsf{z}}}_h) \leqslant s_h(\underline{\mathsf{e}}_h,\underline{\mathsf{e}}_h)^{1/2}s_h(\widehat{\underline{\mathsf{z}}}_h,\widehat{\underline{\mathsf{z}}}_h)^{1/2}$, $s_h(\widehat{\underline{\mathsf{z}}}_h,\widehat{\underline{\mathsf{z}}}_h) = \sum_{T\in\mathcal{T}_h}s_T(I_T^k\underline{z},I_T^k\underline{z})$, and the mesh regularity properties (3) and (4) yield

$$|\mathfrak{T}_1| \leqslant \left\{\|\underline{\mathsf{e}}_h\|_{\varepsilon,h}^2 + s_h(\underline{\mathsf{e}}_h,\underline{\mathsf{e}}_h)\right\}^{1/2} \times \left\{\sum_{T\in\mathcal{T}_h}\left\{\|\underline{\underline{\delta}}_T(\underline{z})\|_T^2 + h_T\|\underline{\underline{\delta}}_T(\underline{z})\|_{\partial T}^2 + (2\mu)^2s_T(I_T^k\underline{z},I_T^k\underline{z})\right\}\right\}^{1/2},$$

with $\underline{\underline{\delta}}_T(\underline{z}) := \underline{\underline{\varsigma}} - \underline{\underline{S}}_T^k \mathsf{L}_T \widehat{\underline{\mathsf{z}}}_h = (2\mu)\nabla_{\rm s}(\underline{z} - \underline{r}_T^k I_T^k \underline{z}) + \lambda(\nabla{\cdot}\underline{z} - \pi_T^k(\nabla{\cdot}\underline{z}))\underline{\underline{I}}_d$. Owing to the estimate (58) on $\underline{\mathsf{e}}_h$, the approximation properties (60) on $\underline{z}$, and the regularity estimate (56), we infer that

$$|\mathfrak{T}_1| \lesssim h^{k+2} B(\underline{u}, k) \left(\|\underline{z}\|_{H^2(\Omega)^d} + \lambda \|\nabla{\cdot}\underline{z}\|_{H^1(\Omega)} \right) \lesssim h^{k+2} B(\underline{u}, k) \|\underline{e}_h\|. \tag{63}$$

Consider now $\mathfrak{T}_2$. Adding $(\underline{\sigma}, \nabla_{\rm s}\underline{z}) - (\underline{f}, \underline{z}) = 0$ and since $l_h(\widehat{\underline{\mathsf{z}}}_h) = \sum_{T\in\mathcal{T}_h} (\underline{f}, \pi_T^k \underline{z})_T$, we infer that

$$\begin{aligned}
\mathcal{E}_h(\widehat{\underline{\mathsf{z}}}_h) = & \sum_{T\in\mathcal{T}_h} \Big\{ (\underline{\sigma}, \nabla_{\rm s}\underline{z})_T - (2\mu)(\underline{\underline{E}}_T^k \mathsf{L}_T \widehat{\underline{\mathsf{u}}}_h, \underline{\underline{E}}_T^k \mathsf{L}_T \widehat{\underline{\mathsf{z}}}_h)_T - \lambda(D_T^k \mathsf{L}_T \widehat{\underline{\mathsf{u}}}_h, D_T^k \mathsf{L}_T \widehat{\underline{\mathsf{z}}}_h) \Big\} \\
& - \sum_{T\in\mathcal{T}_h} (2\mu) s_T(\mathsf{L}_T \widehat{\underline{\mathsf{u}}}_h, \mathsf{L}_T \widehat{\underline{\mathsf{z}}}_h) + \sum_{T\in\mathcal{T}_h} (\underline{f}, \pi_T^k \underline{z} - \underline{z})_T \\
:= & \, \mathfrak{T}_{2,1} + \mathfrak{T}_{2,2} + \mathfrak{T}_{2,3}.
\end{aligned} \tag{64}$$

To bound $\mathfrak{T}_{2,1}$, we observe that $\underline{\underline{E}}_T^k \mathsf{L}_T \widehat{\underline{\mathsf{u}}}_h = \nabla_{\rm s}(\underline{r}_T^k I_T^k \underline{u})$ and $\underline{\underline{E}}_T^k \mathsf{L}_T \widehat{\underline{\mathsf{z}}}_h = \nabla_{\rm s}(\underline{r}_T^k I_T^k \underline{z})$ owing to (16), as well as $D_T^k \mathsf{L}_T \widehat{\underline{\mathsf{u}}}_h = \pi_T^k(\nabla{\cdot}\underline{u})$ and $D_T^k \mathsf{L}_T \widehat{\underline{\mathsf{z}}}_h = \pi_T^k(\nabla{\cdot}\underline{z})$ owing to Proposition 3. Using the orthogonality relation (19), we infer that

$$\mathfrak{T}_{2,1} = \sum_{T\in\mathcal{T}_h} \Big\{ (2\mu)(\nabla_{\rm s}(\underline{u} - \underline{r}_T^k I_T^k \underline{u}), \nabla_{\rm s}(\underline{z} - \underline{r}_T^k I_T^k \underline{z}))_T + \lambda(\nabla{\cdot}\underline{u} - \pi_T^k(\nabla{\cdot}\underline{u}), \nabla{\cdot}\underline{z} - \pi_T^k(\nabla{\cdot}\underline{z}))_T \Big\}.$$

Hence, using the approximation properties (18) and (7) of $\underline{r}_T^k I_T^k$ and π_T^k, respectively, to bound the terms with $\underline{u}$ and using (60a)-(60b) to bound the terms with $\underline{z}$ leads to

$$|\mathfrak{T}_{2,1}| \lesssim h^{k+2} B(\underline{u}, k) \left(\|\underline{z}\|_{H^2(\Omega)^d} + \lambda \|\nabla{\cdot}\underline{z}\|_{H^1(\Omega)} \right). \tag{65}$$

Furthermore, since $s_T(\mathsf{L}_T \widehat{\underline{\mathsf{u}}}_h, \mathsf{L}_T \widehat{\underline{\mathsf{z}}}_h) = s_T(I_T^k \underline{u}, I_T^k \underline{z}) \leqslant s_T(I_T^k \underline{u}, I_T^k \underline{u})^{1/2} s_T(I_T^k \underline{z}, I_T^k \underline{z})^{1/2}$, we infer using (29) and (60c) that

$$|\mathfrak{T}_{2,2}| \lesssim h^{k+2} B(\underline{u}, k) \|\underline{z}\|_{H^2(\Omega)^d}. \tag{66}$$

Finally, since π_T^k is self-adjoint and since $k \geqslant 1$, we infer that $(\underline{f}, \pi_T^k \underline{z} - \underline{z})_T = (\pi_T^k \underline{f} - \underline{f}, \underline{z})_T = (\pi_T^k \underline{f} - \underline{f}, \underline{z} - \pi_T^1 \underline{z})_T$, whence

$$|\mathfrak{T}_{2,3}| \lesssim h^{k+2} \|\underline{f}\|_{H^k(\Omega)^d} \|\underline{z}\|_{H^2(\Omega)^d}. \tag{67}$$

Using (65)–(67) and the regularity estimate (56), we obtain

$$|\mathfrak{T}_2| \lesssim h^{k+2} B(\underline{u}, k) \|\underline{e}_h\|. \tag{68}$$

The estimate (57) follows using (63) and (68) to bound the right-hand side of (61). □

Finally, we infer an L^2-estimate comparing $\underline{u}$ to the global (nonconforming) displacement reconstructions $\underline{r}_h^k \underline{\mathsf{u}}_h$ and $\underline{R}_h^k \underline{\mathsf{u}}_h$ such that $\underline{r}_h^k \underline{\mathsf{u}}_{h|T} = \underline{r}_T^k \mathsf{L}_T \underline{\mathsf{u}}_h$ and $\underline{R}_h^k \underline{\mathsf{u}}_{h|T} = \underline{R}_T^k \mathsf{L}_T \underline{\mathsf{u}}_h$ for all $T \in \mathcal{T}_h$.

Corollary 12 (L^2-estimate on displacement reconstructions)**.** *Under the assumptions of Theorem 11, the following holds:*

$$\max(\|\underline{u} - \underline{r}_h^k \underline{\mathsf{u}}_h\|, \|\underline{u} - \underline{R}_h^k \underline{\mathsf{u}}_h\|) \leqslant C h^{k+2} \left(2\mu \|\underline{u}\|_{H^{k+2}(\mathcal{T}_h)^d} + \lambda \|\nabla{\cdot}\underline{u}\|_{H^{k+1}(\mathcal{T}_h)} \right), \tag{69}$$

where $C > 0$ is a real number independent of λ and h.

Proof. For all $T \in \mathcal{T}_h$, the triangle inequality yields

$$\|\underline{u} - \underline{r}_T^k \mathsf{L}_T \underline{\mathsf{u}}_h\|_T \leqslant \|\underline{u} - \underline{r}_T^k I_T^k \underline{u}\|_T + \|\underline{r}_T^k I_T^k \underline{u} - \underline{r}_T^k \mathsf{L}_T \underline{\mathsf{u}}_h\|_T := \mathfrak{T}_1 + \mathfrak{T}_2,$$

and $\mathfrak{T}_1$ is readily estimated using Lemma 2. To estimate $\mathfrak{T}_2$, we first observe that, for all $\underline{v} \in H^1(T)^d$, we can write $\underline{v} = (\underline{v} - \underline{v}_{\mathrm{RM}}) + \underline{v}_{\mathrm{RM}}$ with $\underline{v}_{\mathrm{RM}} = |T|_d^{-1}(\int_T \underline{v}) + |T|_d^{-1}(\int_T \nabla_{\mathrm{ss}}\underline{v})(\underline{x} - \underline{x}_T)$, where $\underline{x}_T$ denotes the barycenter of T. Since $(\underline{v} - \underline{v}_{\mathrm{RM}}) \in \underline{\mathcal{U}}(T)$, we infer owing to Korn's inequality (11) that $\|\underline{v}\|_T \leqslant C_{\mathrm{K}} h_T \|\nabla_{\mathrm{ss}}\underline{v}\|_T + \|\underline{v}_{\mathrm{RM}}\|_T$, and using Cauchy–Schwarz inequalities leads to

$$\|\underline{v}\|_T \leqslant C_{\mathrm{K}} h_T \|\nabla_{\mathrm{ss}}\underline{v}\|_T + |T|_d^{-1/2} \left| \int_T \underline{v} \right| + |T|_d^{-1/2} h_T \left| \int_T \nabla_{\mathrm{ss}}\underline{v} \right|.$$

Applying this estimate to $\underline{v} = \underline{r}_T^k I_T^k \underline{u} - \underline{r}_T^k \mathsf{L}_T \underline{\mathsf{u}}_h$, recalling (15), and using the Cauchy–Schwarz inequality together with mesh regularity, we infer that

$$|\mathfrak{T}_2| \lesssim h_T \|\underline{\underline{E}}_T^k \mathsf{L}_T(\widehat{\underline{\mathsf{u}}}_h - \underline{\mathsf{u}}_h)\|_T + \|\pi_T^k \underline{u} - \underline{\mathsf{u}}_T\|_T + h_T \sum_{F \in \mathcal{F}_T} h_F^{-1/2} \|\pi_F^k \underline{u} - \underline{\mathsf{u}}_F\|_F := \mathfrak{T}_{2,1} + \mathfrak{T}_{2,2} + \mathfrak{T}_{2,3}.$$

The terms $\mathfrak{T}_{2,1}$ and $\mathfrak{T}_{2,2}$ are estimated using Theorems 8 and 11, respectively. Finally, to estimate $\mathfrak{T}_{2,3}$, we use the triangle inequality and the discrete trace inequality to infer that

$$|\mathfrak{T}_{2,3}| \lesssim h_T \|\mathsf{L}_T \widehat{\underline{\mathsf{u}}}_h - \mathsf{L}_T \underline{\mathsf{u}}_h\|_{\varepsilon,T} + \|\pi_T^k \underline{u} - \underline{\mathsf{u}}_T\|_T,$$

whence the bound on $\|\underline{u} - \underline{r}_h^k \underline{\mathsf{u}}_h\|$ follows from Theorems 8 and 11. To bound $\|\underline{u} - \underline{R}_h^k \underline{\mathsf{u}}_h\|$, we observe that, recalling (26) and using the boundedness of π_T^k,

$$\begin{aligned}\|\underline{u} - \underline{R}_h^k \underline{\mathsf{u}}_h\|_T &\leqslant \|\underline{u} - \underline{r}_h^k \underline{\mathsf{u}}_h\|_T + \|\pi_T^k(\underline{r}_h^k \underline{\mathsf{u}}_h - \underline{u})\|_T + \|\pi_T^k \underline{u} - \underline{\mathsf{u}}_T\|_T \\ &\leqslant 2\|\underline{u} - \underline{r}_h^k \underline{\mathsf{u}}_h\|_T + \|\pi_T^k \underline{u} - \underline{\mathsf{u}}_T\|_T,\end{aligned}$$

whence the conclusion readily follows. □

6 Implementation and numerical study

In this section we discuss implementation aspects and present numerical results. We verify the error estimates derived in the previous section by means of a manufactured exact solution, and we consider the classical Cook's membrane test case. The numerical efficiency in terms of CPU cost is also evaluated.

6.1 Implementation

An important step in the implementation consists in selecting a basis for each of the polynomial spaces that appear in the construction. Let $T \in \mathcal{T}_h$ and denote by $\underline{x}_T$ a point with respect to which T is star-shaped (in the numerical tests, the barycenter of T was used). As a basis for $\mathbb{P}_d^l(T)$, $l \in \{k, k+1\}$, we take, letting $A^l := \{\underline{\alpha} = (\alpha_i)_{1 \leqslant i \leqslant d} \in \mathbb{N}^d \mid \|\underline{\alpha}\|_{\ell^1} \leqslant l\}$,

$$\mathcal{B}_T^l := \left\{ \prod_{i=1}^d \xi_{T,i}^{\alpha_i} \,\middle|\, \underline{\alpha} \in A^l, \quad \xi_{T,i} := \frac{x_i - x_{T,i}}{h_T} \quad \forall 1 \leqslant i \leqslant d \right\}, \tag{70}$$

i.e., the basis $\mathcal{B}_T^l$ is spanned by monomials in the translated and scaled coordinate variables $(\xi_{T,i})_{1 \leqslant i \leqslant d}$. A basis for the polynomial space of vector-valued functions $\mathbb{P}_d^l(T)^d$ is then obtained

by the Cartesian product of $\mathcal{B}_T^l$. Similarly, for all $F \in \mathcal{F}_h$, we can define a basis $\mathcal{B}_F^k$ for $\mathbb{P}_{d-1}^k(F)$ spanned by monomials with respect to a local frame scaled using the face diameter and a point with respect to which F is star-shaped. A basis for $\mathbb{P}_{d-1}^k(F)^d$ is obtained by Cartesian product.

Equation (70) defines hierarchical bases, so that we can construct and evaluate $\mathcal{B}_T^{k+1}$ (required to solve (14)) at quadrature nodes and obtain $\mathcal{B}_T^k$ (used to solve (23)) by simply discarding the highest-order functions. The constraints in (15) are accounted for in problem (14) as follows: the zero-average condition for the displacement is replaced by the requirement that functions vanish at $\underline{x}_T$, and this condition is incorporated by simply discarding the constant function in $\mathcal{B}_T^{k+1}$; the zero-average condition for the skew-symmetric part of the gradient is enforced using a Lagrange multiplier (which is scalar-valued for $d = 2$ and $\mathbb{R}^3$-valued for $d = 3$). Moreover, the homogeneous Dirichlet boundary condition is also enforced by means of a Lagrange multiplier in $\mathbb{P}_{d-1}^k(F)^d$ for all $F \in \mathcal{F}_h^{\mathrm{b}}$.

Concerning numerical integration, in the two-dimensional case we can exploit the decomposition of elements into triangles and use standard quadrature rules. In our implementation, we have used the quadrature rules available in GetFem++ [26]. In the three-dimensional case, this is also possible provided the faces of the elements are triangles or quadrangles yielding pyramidal sub-elements for which standard cubature rules are available. If this is not the case, a simplicial decomposition of the element can be considered, usually implying an increase in the number of quadrature nodes. Similarly, numerically integrating on the mesh faces is straightforward in two space dimensions and for elements with triangular or quadrangular faces in three space dimensions. For more general polygonal faces in three space dimensions, triangulating the face may be required.

6.2 Convergence and computational cost

To verify the estimates of Theorems 8 and 11, we solve the two-dimensional, pure-displacement problem with $\mu = 1$, $\lambda \in \{1, 1000\}$, displacement $\underline{u} = (u_1, u_2)$ such that

$$u_1 = \sin(\pi x_1)\sin(\pi x_2) + \frac{1}{2\lambda}x_1, \qquad u_2 = \cos(\pi x_1)\cos(\pi x_2) + \frac{1}{2\lambda}x_2, \tag{71}$$

and load $\underline{f} = (f_1, f_2)$ such that

$$f_1 = 2\pi^2 \sin(\pi x_1)\sin(\pi x_2), \qquad f_2 = 2\pi^2 \cos(\pi x_1)\cos(\pi x_2).$$

The solution (71) has vanishing divergence in the limit $\lambda \to +\infty$. This, together with the fact that $\underline{f}$ does not depend on λ, make this test case suitable to check numerically that the estimates (44) and (57) are indeed uniform in λ. We consider the three families of meshes depicted in Figure 2: the matching triangular and Kershaw mesh families of [21] and the (predominantly) hexagonal mesh family considered in [16, Section 4.2.3]. The stress error is the one estimated in Theorem 8, and the displacement error is estimated as $\|\underline{u} - \underline{R}_h^k \underline{\mathbf{u}}_h\|$, cf. Corollary 12. The convergence rates displayed in Figure 3 and 4 for $\lambda = 1$ and $\lambda = 1000$, respectively, are in agreement with the theoretical predictions. The slight superconvergence observed for the Kershaw mesh family is due to the fact that the mesh regularity increases when refining. As predicted, the error does not depend on λ.

To check the performance of the proposed method in terms of CPU time, we have instrumented our code in the spirit of [15] to separately measure (i) the *assembly time* τ_{ass}, accounting for the construction of the local contributions to the bilinear form a_h (cf. (38)),

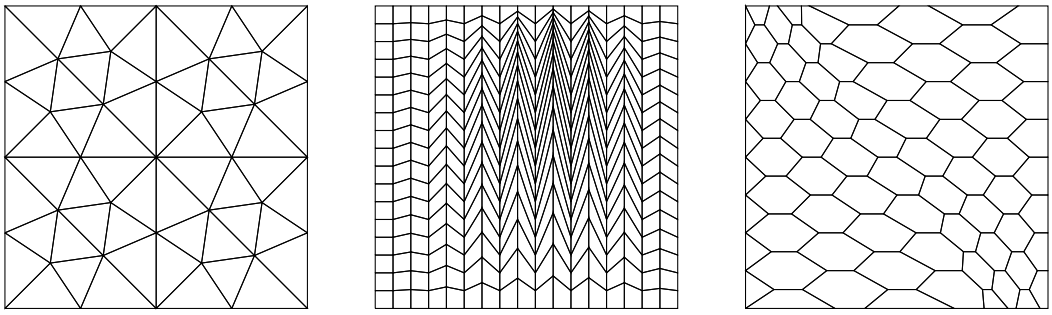

Figure 2: Triangular, Kershaw, and hexagonal meshes for the numerical example of Section 6

the local elimination of cell unknowns, and the assembly into a global matrix; (ii) the *solution time* τ_{sol} corresponding to the solution of the global linear system. Local computations are based on the linear algebra facilities provided by the Eigen3 library [19]. The linear systems corresponding to problems (14), (23), and to the L^2-orthogonal projectors π_T^k and π_F^k are solved using the robust Cholesky factorization available in Eigen3. The global system (involving face unknowns only) is solved using SuperLU [11] through the PETSc 3.4 interface [2]. The tests have been run sequentially on a laptop computer powered by an Intel Core i7-3520 CPU running at 2.90 GHz and equipped with 8Gb of RAM.

To check how the more elaborate local computations (with respect, e.g., to standard finite elements) affect the overall CPU cost, we plot in Figure 5 the ratio $\tau_{\mathrm{ass}}/\tau_{\mathrm{sol}}$ as a function of $\mathrm{card}(\mathcal{F}_h)$. We consider the triangular and hexagonal mesh families for which N_∂ (cf. (4)) is respectively the smallest and the largest. It can be observed that, when refining the mesh, the ratio $\tau_{\mathrm{ass}}/\tau_{\mathrm{sol}}$ rapidly decreases as a result of having (approximately) $\tau_{\mathrm{ass}} \propto \mathrm{card}(\mathcal{F}_h)$ and $\tau_{\mathrm{sol}} \propto \mathrm{card}(\mathcal{F}_h)^{3/2}$. This means that, in large test cases, the local computations can be expected to have a negligible impact on the global CPU time.

Figures 6 and 7 depict the stress and displacement errors as a function of the total CPU time $\tau_{\mathrm{tot}} := \tau_{\mathrm{ass}} + \tau_{\mathrm{sol}}$. This representation is included to provide a fair basis of future comparison with other methods. As expected from the regularity of the exact solution (71), the highest-order computation provides in all the cases the best precision for a given CPU time as well as the largest reduction rate for the error.

6.3 Cook's membrane test case

We next consider a bending dominated test case widely used in the mechanical engineering literature and referred to as Cook's membrane; cf. Figure 8 for a description of the domain and of the boundary conditions. Following [1], we take a quasi-incompressible material with $\mu = 0.375$ and $\lambda = 7.5\times10^6$. The load F (cf. again Figure 8) is uniform and has unitary resultant. We monitor the following quantities at the middle point A of coordinates $\underline{x}_A = (48, 52)$ of the right side of the domain: (i) the displacement, measured using the piecewise polynomial, vector-valued fields $\underline{u}_h = (u_{h,1}, u_{h,2}) \in \mathbb{P}_d^k(\mathcal{T}_h)^d$ and $\breve{\underline{u}}_h = (\breve{u}_{h,1}, \breve{u}_{h,2}) \in \mathbb{P}_d^{k+1}(\mathcal{T}_h)^d$ such that $\underline{u}_{h|T} = \underline{\mathbf{u}}_T$ for all $T \in \mathcal{T}_h$ and $\breve{\underline{u}}_h = \underline{R}_h^k \underline{\mathbf{u}}_h$ (cf. Corollary 12) and (ii) the pressure $p_h(\underline{x}_A)$ measured by the quantity $\lambda D_T^k \mathsf{L}_T \underline{\mathbf{u}}_h$ where T denotes one mesh element such that $A \in \partial T$ (when two such elements exist, we arbitrarily choose one of them). The problem is solved on triangular, Kershaw, and (predominantly) hexagonal mesh sequences obtained by mapping the meshes depicted in Figure 2 onto the domain represented in Figure 8. Since no

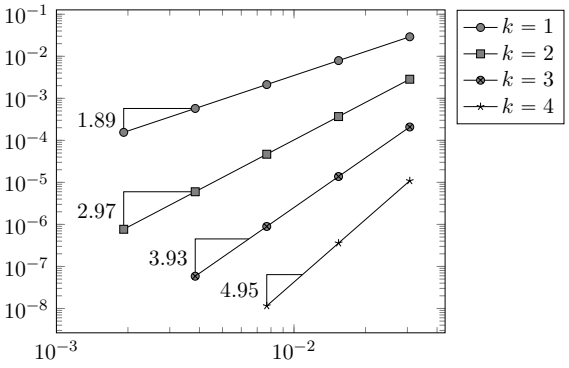

(a) Stress error, triangular mesh family

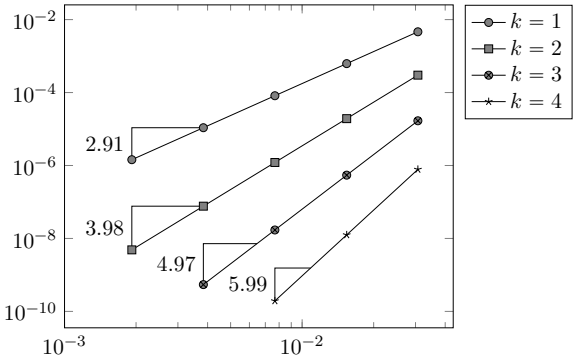

(b) Displacement error, triangular mesh family

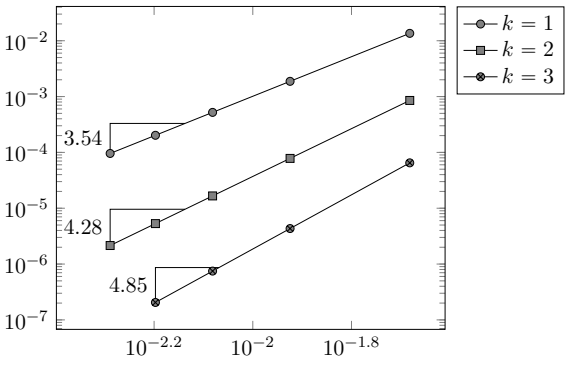

(c) Stress error, Kershaw mesh family

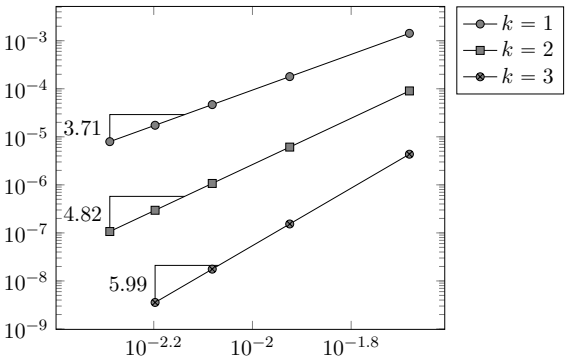

(d) Displacement error, Kershaw mesh family

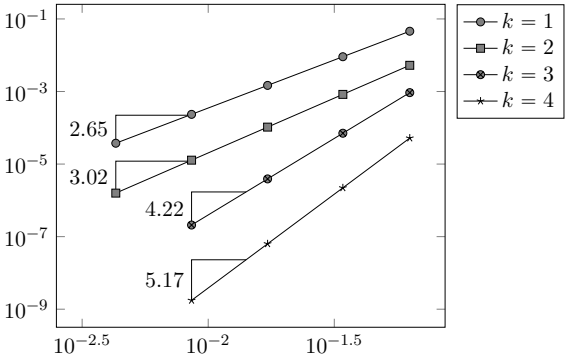

(e) Stress error, hexagonal mesh family

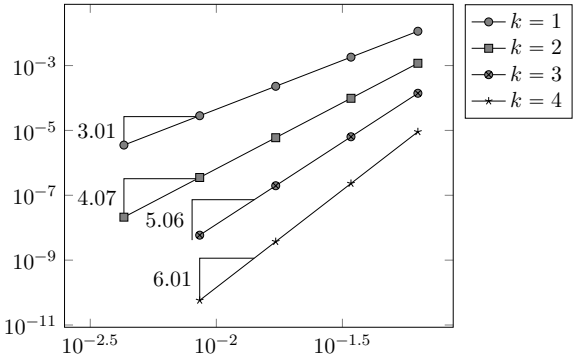

(f) Displacement error, hexagonal mesh family

Figure 3: Errors vs. h for $\lambda = 1$

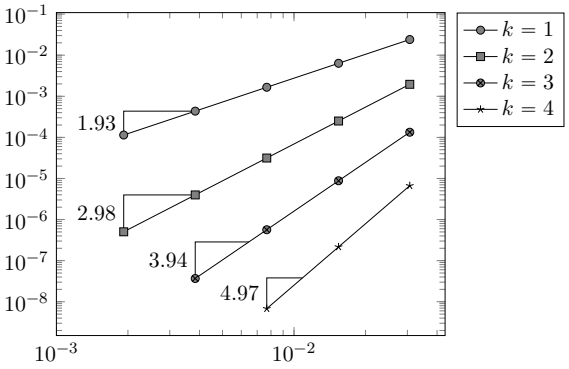

(a) Stress error, triangular mesh family

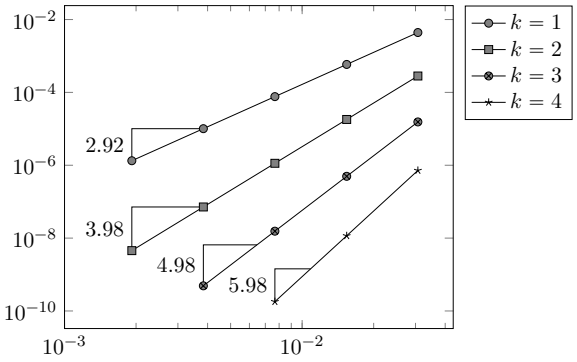

(b) Displacement error, triangular mesh family

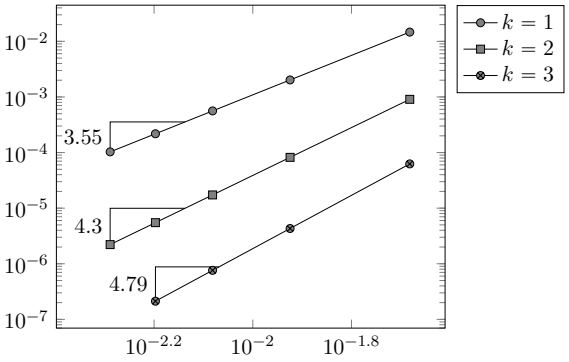

(c) Stress error, Kershaw mesh family

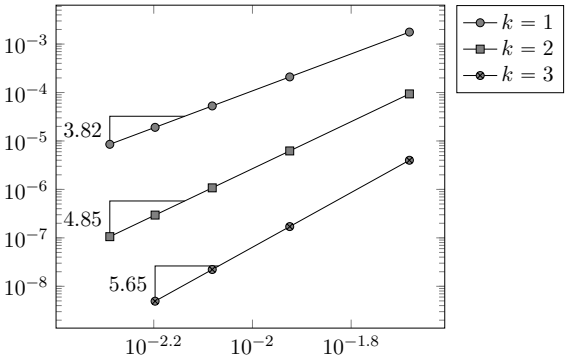

(d) Displacement error, Kershaw mesh family

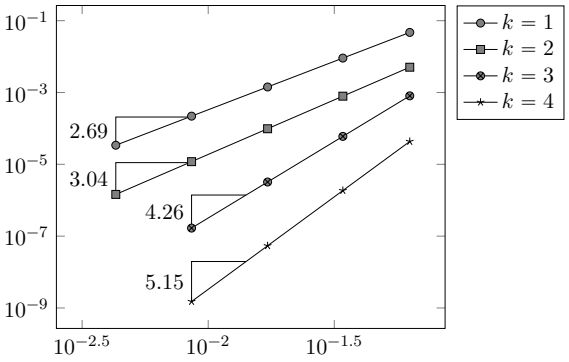

(e) Stress error, hexagonal mesh family

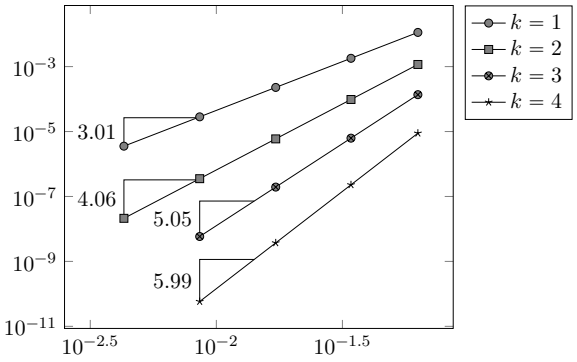

(f) Displacement error, hexagonal mesh family

Figure 4: Errors vs. h for $\lambda = 10^3$

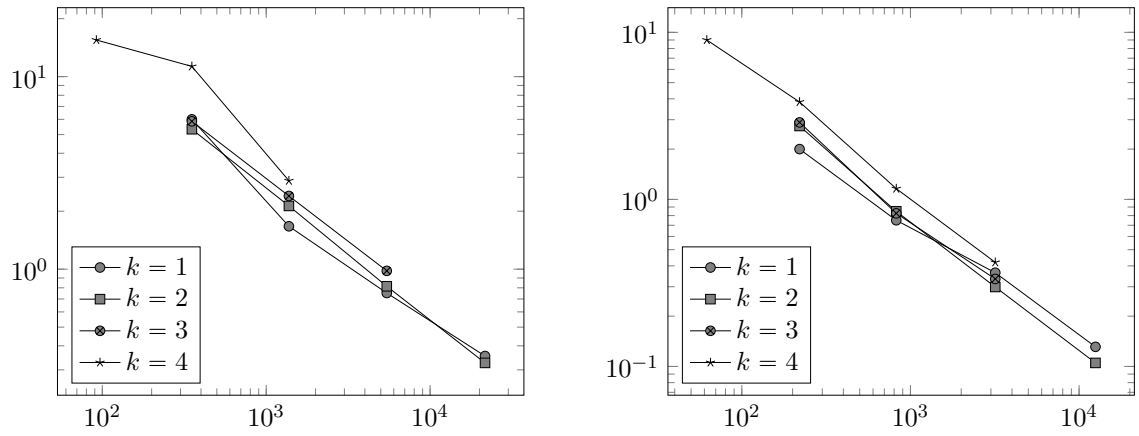

(a) Triangular mesh family (b) Hexagonal mesh family

Figure 5: $\tau_{\text{ass}}/\tau_{\text{sol}}$ vs. $\text{card}(\mathcal{F}_h)$

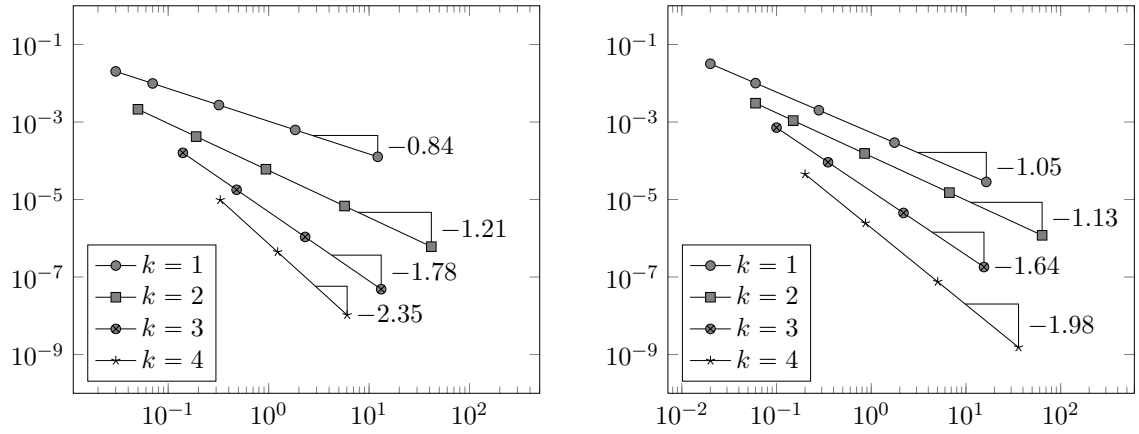

(a) Triangular mesh family (b) Hexagonal mesh family

Figure 6: Stress error vs. τ_{tot} (s)

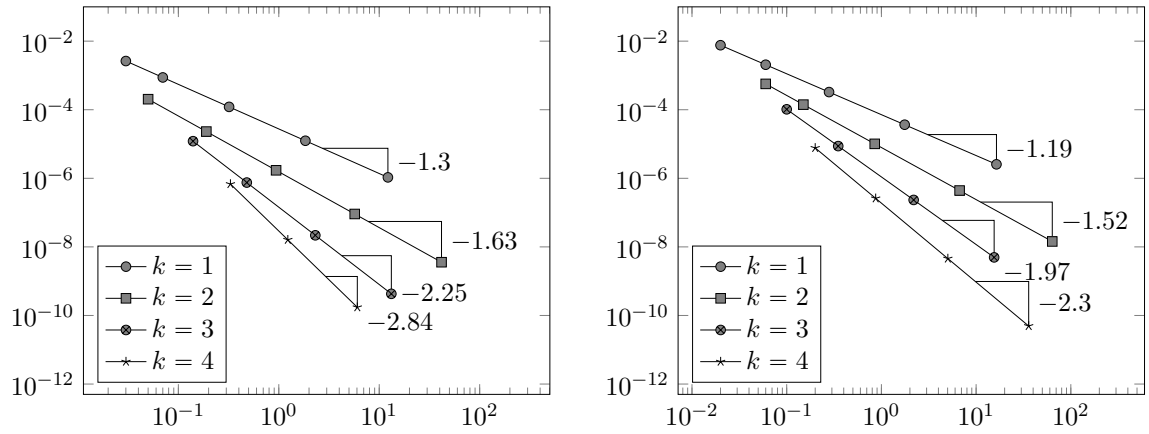

(a) Triangular mesh family (b) Hexagonal mesh family

Figure 7: Displacement error vs. τ_{tot} (s)

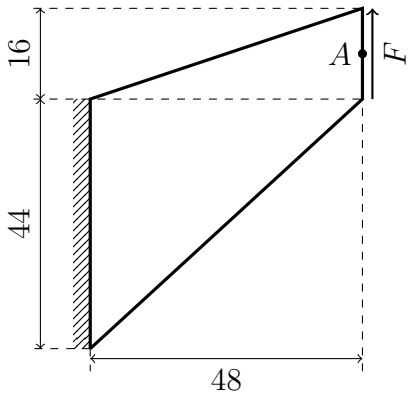

Figure 8: Configuration for Cook's membrane test case.

Table 1: Cook's test case (cf. Section 6.3), triangular mesh family

(a) $k = 1$

$\mathrm{card}(\mathcal{T}_h)$	$\mathrm{card}(\mathcal{F}_h)$	$u_{h,1}(\underline{x}_A)$	$\breve{u}_{h,1}(\underline{x}_A)$	$u_{h,2}(\underline{x}_A)$	$\breve{u}_{h,2}(\underline{x}_A)$	$p_h(\underline{x}_A)$
56	92	-7.390	-7.414	16.712	16.717	$5.123 \cdot 10^{-2}$
224	352	-7.312	-7.319	16.566	16.560	$5.860 \cdot 10^{-2}$
896	1,376	-7.279	-7.282	16.498	16.496	$6.614 \cdot 10^{-2}$
3,584	5,440	-7.265	-7.265	16.468	16.468	$6.957 \cdot 10^{-2}$
14,336	21,632	-7.255	-7.255	16.449	16.449	$7.051 \cdot 10^{-2}$

(b) $k = 2$

$\mathrm{card}(\mathcal{T}_h)$	$\mathrm{card}(\mathcal{F}_h)$	$u_{h,1}(\underline{x}_A)$	$\breve{u}_{h,1}(\underline{x}_A)$	$u_{h,2}(\underline{x}_A)$	$\breve{u}_{h,2}(\underline{x}_A)$	$p_h(\underline{x}_A)$
56	92	-7.320	-7.325	16.586	16.571	$6.219 \cdot 10^{-2}$
224	352	-7.282	-7.283	16.501	16.498	$6.911 \cdot 10^{-2}$
896	1,376	-7.268	-7.268	16.474	16.474	$7.077 \cdot 10^{-2}$
3,584	5,440	-7.264	-7.264	16.467	16.467	$7.086 \cdot 10^{-2}$
14,336	21,632	-7.260	-7.260	16.460	16.460	$7.093 \cdot 10^{-2}$

analytical solution is available for this test case, we use as reference quantities those obtained for $k = 2$ on the finest triangular mesh composed of 14,336 elements:

$$\breve{u}_{h,1}(\underline{x}_A) = -7.2596{\times}10^{0} \qquad \breve{u}_{h,2}(\underline{x}_A) = 1.6460{\times}10^{1} \qquad p_h(\underline{x}_A) = 7.0928{\times}10^{-2}.$$

The results collected in Tables 1–3 show that the proposed method delivers accurate results even on coarser meshes, and that the behavior of the solution is very well-captured using few elements. As expected, the difference between the approximations $\underline{u}_h$ and $\breve{\underline{u}}_h$ of the displacement becomes negligible for sufficiently refined meshes. A comparison of the displacement values for different meshes and polynomial degrees is presented in Figure 9. Finally, the solutions obtained for $k = 1$ on the coarsest, intermediate and finest hexagonal mesh refinement levels are plotted in Figure 10. One can appreciate from Figure 10 that a reasonably accurate solution is obtained even with very few (22) elements and $k = 1$. The interface jumps in the displacement field that are visible in left panel of Figure 10 become rapidly negligible when refining the mesh, as reflected in the central and right panels.

Table 2: Cook's test case (cf. Section 6.3), Kershaw mesh family

(a) $k = 1$

$\mathrm{card}(\mathcal{T}_h)$	$\mathrm{card}(\mathcal{F}_h)$	$u_{h,1}(\underline{x}_A)$	$\breve{u}_{h,1}(\underline{x}_A)$	$u_{h,2}(\underline{x}_A)$	$\breve{u}_{h,2}(\underline{x}_A)$	$p_h(\underline{x}_A)$
289	612	-7.334	-7.343	16.590	16.594	$6.855 \cdot 10^{-2}$
1,156	2,380	-7.291	-7.296	16.513	16.516	$7.011 \cdot 10^{-2}$
2,601	5,304	-7.280	-7.282	16.494	16.494	$7.068 \cdot 10^{-2}$
4,624	9,384	-7.273	-7.275	16.482	16.483	$7.068 \cdot 10^{-2}$
7,225	14,620	-7.270	-7.270	16.476	16.476	$7.079 \cdot 10^{-2}$

(b) $k = 2$

$\mathrm{card}(\mathcal{T}_h)$	$\mathrm{card}(\mathcal{F}_h)$	$u_{h,1}(\underline{x}_A)$	$\breve{u}_{h,1}(\underline{x}_A)$	$u_{h,2}(\underline{x}_A)$	$\breve{u}_{h,2}(\underline{x}_A)$	$p_h(\underline{x}_A)$
289	612	-7.315	-7.316	16.547	16.546	$7.112 \cdot 10^{-2}$
1,156	2,380	-7.285	-7.286	16.499	16.499	$7.088 \cdot 10^{-2}$
2,601	5,304	-7.276	-7.276	16.484	16.484	$7.086 \cdot 10^{-2}$
4,624	9,384	-7.267	-7.267	16.471	16.471	$7.084 \cdot 10^{-2}$
7,225	14,620	-7.264	-7.264	16.466	16.466	$7.086 \cdot 10^{-2}$

Table 3: Cook's test case (cf. Section 6.3), hexagonal mesh family

(a) $k = 1$

$\mathrm{card}(\mathcal{T}_h)$	$\mathrm{card}(\mathcal{F}_h)$	$u_{h,1}(\underline{x}_A)$	$\breve{u}_{h,1}(\underline{x}_A)$	$u_{h,2}(\underline{x}_A)$	$\breve{u}_{h,2}(\underline{x}_A)$	$p_h(\underline{x}_A)$
22	62	-7.275	-7.326	16.563	16.621	$4.321 \cdot 10^{-2}$
76	220	-7.270	-7.302	16.510	16.526	$5.554 \cdot 10^{-2}$
280	824	-7.268	-7.284	16.485	16.493	$6.457 \cdot 10^{-2}$
1,072	3,184	-7.265	-7.270	16.472	16.475	$6.895 \cdot 10^{-2}$
4,192	12,512	-7.261	-7.262	16.463	16.464	$7.036 \cdot 10^{-2}$

(b) $k = 2$

$\mathrm{card}(\mathcal{T}_h)$	$\mathrm{card}(\mathcal{F}_h)$	$u_{h,1}(\underline{x}_A)$	$\breve{u}_{h,1}(\underline{x}_A)$	$u_{h,2}(\underline{x}_A)$	$\breve{u}_{h,2}(\underline{x}_A)$	$p_h(\underline{x}_A)$
22	62	-7.291	-7.264	16.533	16.497	$5.975 \cdot 10^{-2}$
76	220	-7.275	-7.283	16.491	16.493	$6.808 \cdot 10^{-2}$
280	824	-7.267	-7.269	16.473	16.475	$7.120 \cdot 10^{-2}$
1,072	3,184	-7.261	-7.261	16.462	16.462	$7.088 \cdot 10^{-2}$
4,192	12,512	-7.259	-7.259	16.459	16.459	$7.084 \cdot 10^{-2}$

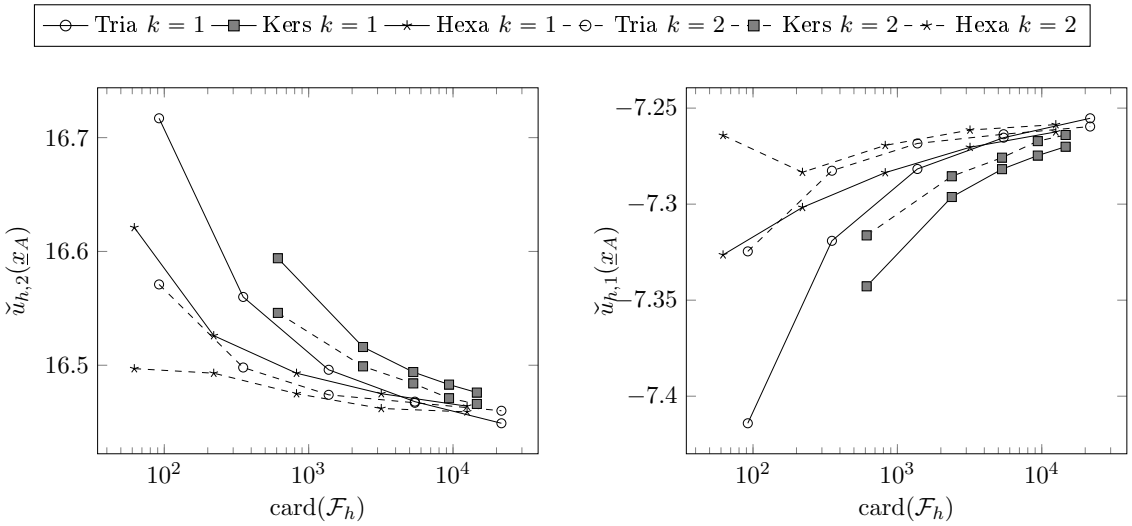

Figure 9: Vertical (left) and horizontal (right) displacement at point A (cf. Figure 8) for Cook's membrane test case described in Section 6.3. The tests were run with $k = 1$ (solid lines), $k = 2$ (dashed lines) and meshes obtained by mapping the meshes of Figure 2 onto the domain depicted in Figure 8.

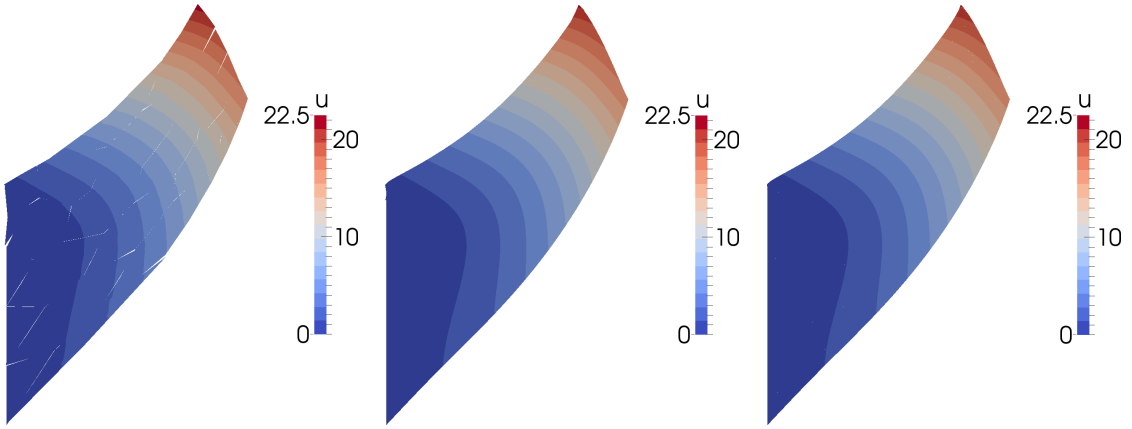

(a) 22 elements (b) 280 elements (c) 4,192 elements

Figure 10: Deformed configuration for the coarsest, intermediate, and finest hexagonal meshes for Cook's test case described in Section 6.3. The color represents the magnitude of the displacement field $\underline{R}_h^k \underline{\mathbf{u}}_h$ (cf. Corollary 12).

References

[1] F. Auricchio, L. Beirão da Veiga, C. Lovadina, and A. Reali. An analysis of some mixed-enhanced finite element for plane linear elasticity. *CMAME*, 194:2947–2968, 2005.

[2] S. Balay, J. Brown, K. Buschelman, W. D. Gropp, D. Kaushik, M. G. Knepley, L. Curfman McInnes, B. F. Smith, and H. Zhang. PETSc Web page. `http://www.mcs.anl.gov/petsc`, 2011.

[3] M. Bebendorf. A note on the Poincaré inequality for convex domains. *Z. Anal. Anwendungen*, 22(4):751–756, 2003.

[4] L. Beirão da Veiga, F. Brezzi, and L. D. Marini. Virtual elements for linear elasticity problems. *SIAM J. Numer. Anal.*, 2(51):794–812, 2013.

[5] L. Beirão da Veiga, V. Gyrya, K. Lipnikov, and G. Manzini. Mimetic finite difference method for the Stokes problem on polygonal meshes. *J. Comput. Phys.*, 228(19):7215–7232, 2009.

[6] L. Beirão Da Veiga. A mimetic discretization method for linear elasticity. *M2AN Math. Model. Numer. Anal.*, 44(2):231–250, 2010.

[7] S. C. Brenner. Korn's inequalities for piecewise H^1 vector fields. *Math. Comp.*, 73(247):1067–1087 (electronic), 2004.

[8] S. C. Brenner and L.-Y. Sung. Linear finite element methods for planar linear elasticity. *Math. Comp.*, 59(200):321–338, 1992.

[9] B. Cockburn, J. Gopalakrishnan, and R. Lazarov. Unified hybridization of discontinuous Galerkin, mixed, and continuous Galerkin methods for second order elliptic problems. *SIAM J. Numer. Anal.*, 47(2):1319–1365, 2009.

[10] M. Crouzeix and P.-A. Raviart. Conforming and nonconforming finite element methods for solving the stationary Stokes equations. *RAIRO Modél. Math. Anal. Num.*, 7(3):33–75, 1973.

[11] J. W. Demmel, S. C. Eisenstat, J. R. Gilbert, X. S. Li, and J. W. H. Liu. A supernodal approach to sparse partial pivoting. *SIAM J. Matrix Analysis and Applications*, 20(3):720–755, 1999.

[12] D. A. Di Pietro and A. Ern. *Mathematical aspects of discontinuous Galerkin methods*, volume 69 of *Mathématiques & Applications*. Springer-Verlag, Berlin, 2012.

[13] D. A. Di Pietro and A. Ern. A family of arbitrary order mixed methods for heterogeneous anisotropic diffusion on general meshes. Submitted. Preprint hal-00918482, 2013.

[14] D. A. Di Pietro, A. Ern, and S. Lemaire. An arbitrary-order and compact-stencil discretization of diffusion on general meshes based on local reconstruction operators. *Comput. Methods Appl. Math.*, 2014. Published online. DOI 10.1515/cmam-2014-0018.

[15] D. A. Di Pietro, J.-M. Gratien, and C. Prud'homme. A domain-specific embedded language in C++ for lowest-order discretizations of diffusive problems on general meshes. *BIT Numerical Mathematics*, 53(1):111–152, 2013.

[16] D. A. Di Pietro and S. Lemaire. An extension of the Crouzeix–Raviart space to general meshes with application to quasi-incompressible linear elasticity and Stokes flow. *Math. Comp.*, 2014. Accepted for publication. Preprint hal-00753660.

[17] A. V. C. Duarte, E. G. D. do Carmo, and F. A. Rochinha. Consistent discontinuous finite elements in elastodynamics. *Comput. Methods Appl. Mech. Engrg.*, 190(1-2):193–223, 2000.

[18] T. Dupont and R. Scott. Polynomial approximation of functions in Sobolev spaces. *Math. Comp.*, 34(150):441–463, 1980.

[19] G. Guennebaud and B. Jacob. Eigen v3. `http://eigen.tuxfamily.org`, 2010.

[20] P. Hansbo and M. G. Larson. Discontinuous Galerkin and the Crouzeix–Raviart element: application to elasticity. *M2AN Math. Model. Numer. Anal.*, 37(1):63–72, 2003.

[21] R. Herbin and F. Hubert. Benchmark on discretization schemes for anisotropic diffusion problems on general grids. In R. Eymard and J.-M. Hérard, editors, *Finite Volumes for Complex Applications V*, pages 659–692. John Wiley & Sons, 2008.

[22] C. O. Horgan. Korn's inequalities and their applications in continuum mechanics. *SIAM Rev.*, 37:491–511, 1995.

[23] C. O. Horgan and L. E. Payne. On inequalities of Korn, Friedrichs, and Babuška–Aziz. *Arch. Rational Mech. Anal.*, 82:165–179, 1983.

[24] Kwang-Yeon Kim. Guaranteed a posteriori error estimator for mixed finite element methods of linear elasticity with weak stress symmetry. *SIAM J. Numer. Anal.*, 48(6):2364–2385, 2011.

[25] K. Lipnikov and G. Manzini. A high-order mimetic method on unstructured polyhedral meshes for the diffusion equation. *J. Comput. Phys.*, 272:360–385, 2014.

[26] Y. Renard and J. Pommier. Getfem++. `http://download.gna.org/getfem/html/homepage/`, 2004.

[27] S.-C. Soon, B. Cockburn, and H. K. Stolarski. A hybridizable discontinuous Galerkin method for linear elasticity. *Internat. J. Numer. Methods Engrg.*, 80(8):1058–1092, 2009.

[28] A. Tabarraei and N. Sukumar. Application of polygonal finite elements in linear elasticity. *Int. J. Comput. Methods*, 3, 2006.

[29] Junping Wang and Xiu Ye. A weak Galerkin finite element method for second-order elliptic problems. *J. Comput. Appl. Math.*, 241:103–115, 2013.